

## Recent results using the EFT of LSS

Baldauf, Mercolli & MZ 1507.02256

Baldauf, Schaan & MZ 1505.07098, 1507.02255

Mirbabayi & MZ 1511.01889

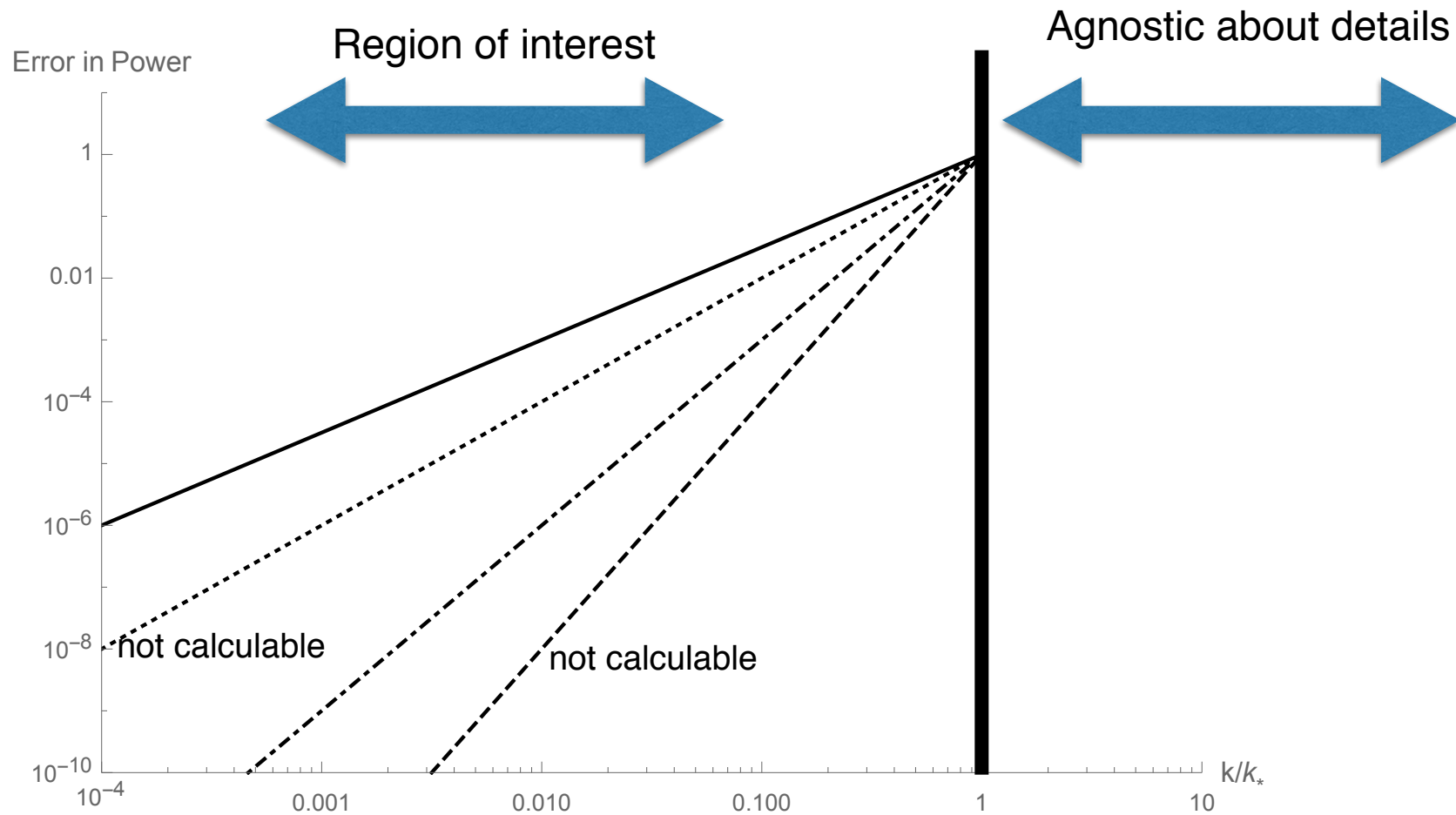
Baldauf, Mirbabayi, Simonovic & MZ 1602.00674

## EFT of LSS

- Study regime of small corrections
- Characterize terms
- Calculable vs non-calculable (counter terms)
- How many terms to achieve a desired accuracy?
- What is the relation between results for different statistics

## Properties of the EFT

- Write all terms consistent with symmetries: Equivalence principle
- Non-locality in time



There are contributions whose size cannot be computed within the large scale theory, they depend on the details of the small scale dynamics. However there  $k$  dependence is known.

## Examples:

$\delta_0(\mathbf{k})$       Initial conditions

$$\delta^{(2)}(\mathbf{k}) = \int_p \left[ \frac{3}{14} \left( 1 - \frac{(\mathbf{p}_1 \cdot \mathbf{p}_2)^2}{p_1^2 p_2^2} \right) + \frac{1}{2} \frac{\mathbf{k} \cdot \mathbf{p}_2}{p_1^2} \frac{\mathbf{k} \cdot \mathbf{p}_2}{p_2^2} \right] \delta_0(\mathbf{p}_1) \delta_0(\mathbf{p}_2) \quad \text{First correction}$$

$$\delta^{ct(1)}(\mathbf{k}) = l_1^2 \mathbf{k}^2 \delta_0(\mathbf{k}) + l_1^2 \int_p \frac{\mathbf{k} \cdot \mathbf{p}_1}{p_1^2} \frac{\mathbf{k} \cdot \mathbf{p}_2}{p_2^2} p_1^2 \delta_0(\mathbf{p}_1) \delta_0(\mathbf{p}_2) \quad \text{first “un-calculable” piece (starts linear)}$$

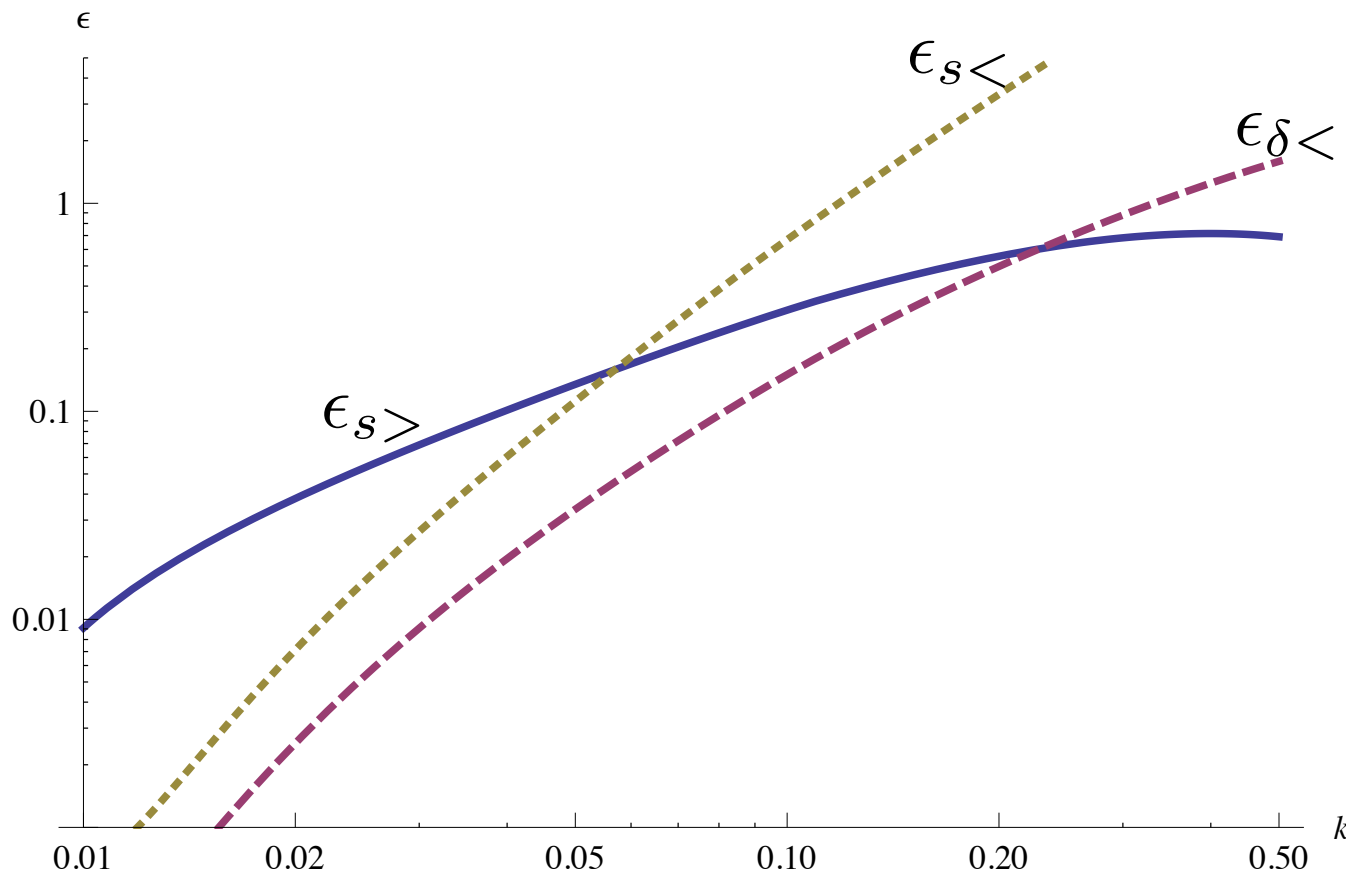
$$\delta^{ct(2)}(\mathbf{k}) = \int_p \left[ l_{21}^2 \mathbf{k}^2 + l_{22}^2 \mathbf{k}^2 \left( 1 - \frac{(\mathbf{p}_1 \cdot \mathbf{p}_2)^2}{p_1^2 p_2^2} \right) + l_{23}^2 \frac{\mathbf{k} \cdot \mathbf{p}_1}{p_1^2} \frac{\mathbf{k} \cdot \mathbf{p}_2}{p_2^2} \frac{\mathbf{p}_1 \cdot \mathbf{p}_2}{p_1^2 p_2^2} \right] \delta_0(\mathbf{p}_1) \delta_0(\mathbf{p}_2) \quad \text{“un-calculable” pieces that starts quadratic}$$

# Corrections to power spectrum for scale-free initial conditions

$P(k) \propto k^n$	$P_{\text{correction}}/P \propto \left(\frac{k}{k_*}\right)^{n+3} \propto k^{1.5}$	Calculable
	$+ \left(\frac{k}{k_*}\right)^2$	“Not Calculable”
	$+ \left(\frac{k}{k_*}\right)^{2(n+3)} \propto k^3$	Calculable
	$+ \left(\frac{k}{k_*}\right)^2 \left(\frac{k}{k_*}\right)^{(n+3)} \propto k^{3.5}$	“Not Calculable”
	$+ \left(\frac{k}{k_*}\right)^4$	“Not Calculable”
	$+ \left(\frac{k}{k_*}\right)^{3(n+3)} \propto k^{4.5}$	Calculable

## Linear theory and scales in our Universe

- Matter radiation equality
- BAO scale
- Neutrino free streaming



$$\epsilon_{s<} = k^2 \int_0^k d^3q \frac{P(q)}{q^2}$$

Motions produced by modes of larger scale than k

$$\epsilon_{s>} = k^2 \int_k^\infty d^3q \frac{P(q)}{q^2}$$

Motions produced by modes of smaller scale than k

$$\epsilon_{\delta<} = \int_0^k d^3q P(q)$$

Tides produced by modes of larger scale than k

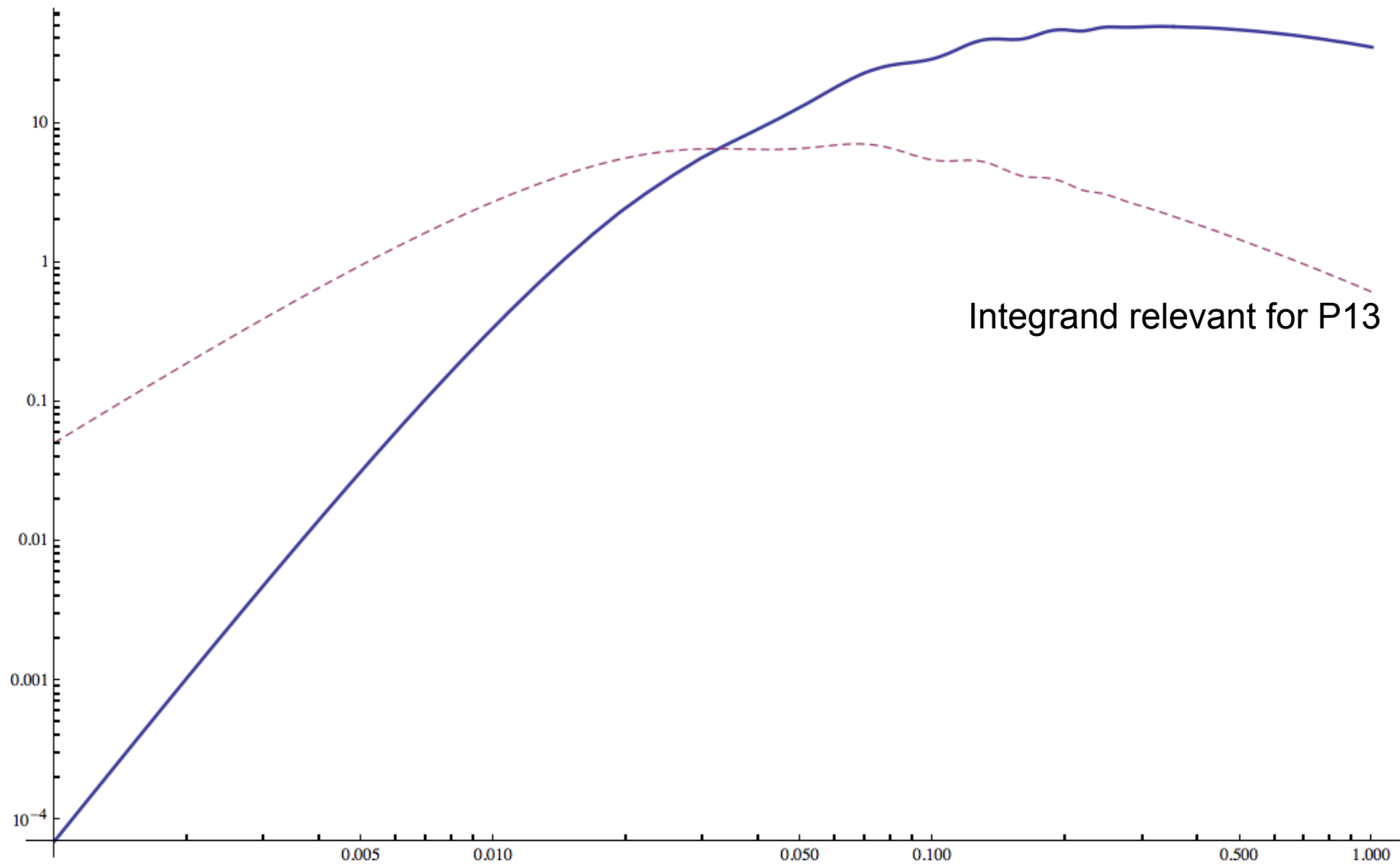
$$\epsilon_{\delta>} = \int_k^\infty d^3q P(q)$$

Does not appear.

# Contributions to the displacement field loop power spectrum

We expect UV sensitivity to be more important as we go to higher loops

Arbitrary normalization



# EFT of LSS directly in Eulerian space

$$\partial_\tau \delta + \partial_i [(1 + \delta)v^i] = \partial_i u^i ,$$

$$\partial_\tau v^i + \mathcal{H}v^i + \partial^i \phi + v^j \partial_j v^i = -\frac{1}{a\rho} \partial_j \tau^{ij}$$

$$\delta = \delta_{(1)} + \delta_{(2)} + \delta_{(3)} + \delta_{(4)} + \delta_{(5)} + \dots$$

$$\Delta \phi = \frac{3}{2} \mathcal{H}^2 \Omega_m \delta .$$

$$\tau_\theta \equiv -\partial_i \left[ \frac{1}{a\rho} \partial_j \tau^j \right] = \tau_\theta^{\text{det}} + \tau_\theta^{\text{stoch}}$$

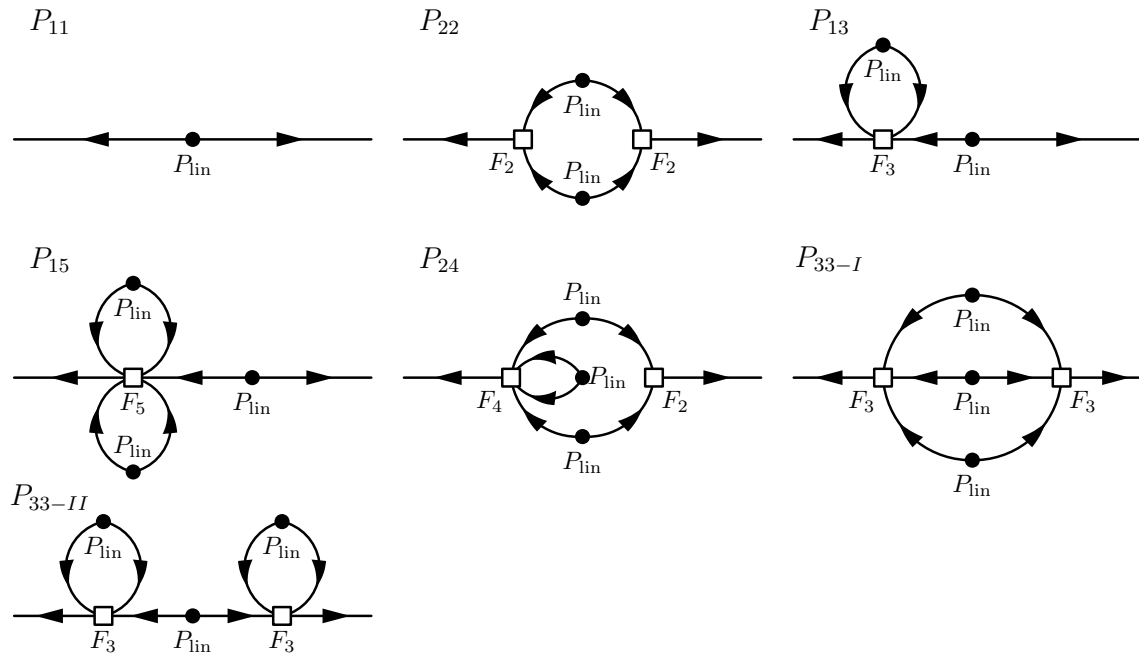
$$\tau_\theta^{\text{det}} = \tau_\theta^{\text{det}} [\partial_i \partial_j \bar{\phi}] .$$

$$\tau_\theta^{\text{det}} \Big|_{\text{LO}} = -d^2 \Delta \delta_{(1)} = -d^2 \Delta \Delta \bar{\phi}_{(1)}$$

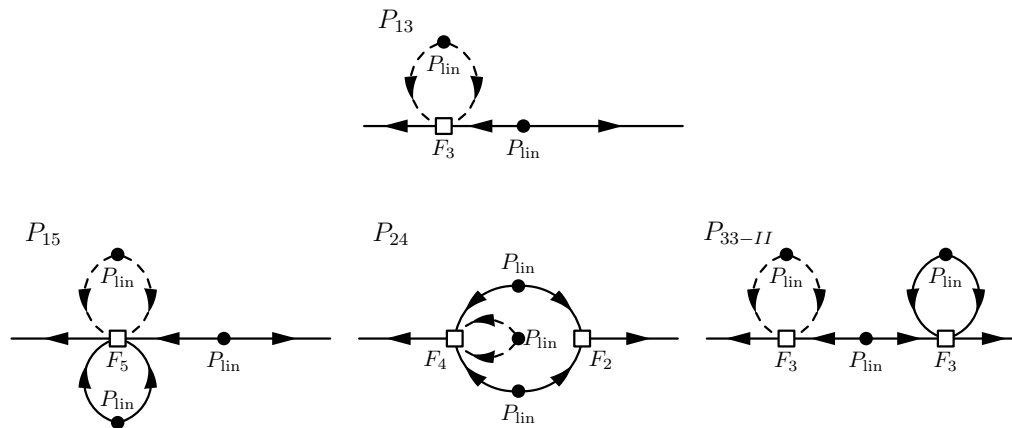
$$\tau_\theta^{\text{det}} \Big|_{\text{NLO}} = -d^2 \Delta [\delta_{(1)} + \delta_{(2)}] - e_1 \Delta \delta_{(1)}^2 - e_2 \Delta (s_{ij(1)} s_{(1)}^{ij}) - e_3 \partial_i s_{(1)}^{ij} \partial_j \delta_{(1)} ,$$

$$s_{ij} = \left( \partial_i \partial_j - \frac{1}{3} \delta_{ij}^{(\text{K})} \Delta \right) \bar{\phi} .$$

# Diagrams:



# Leading UV sensitivity:



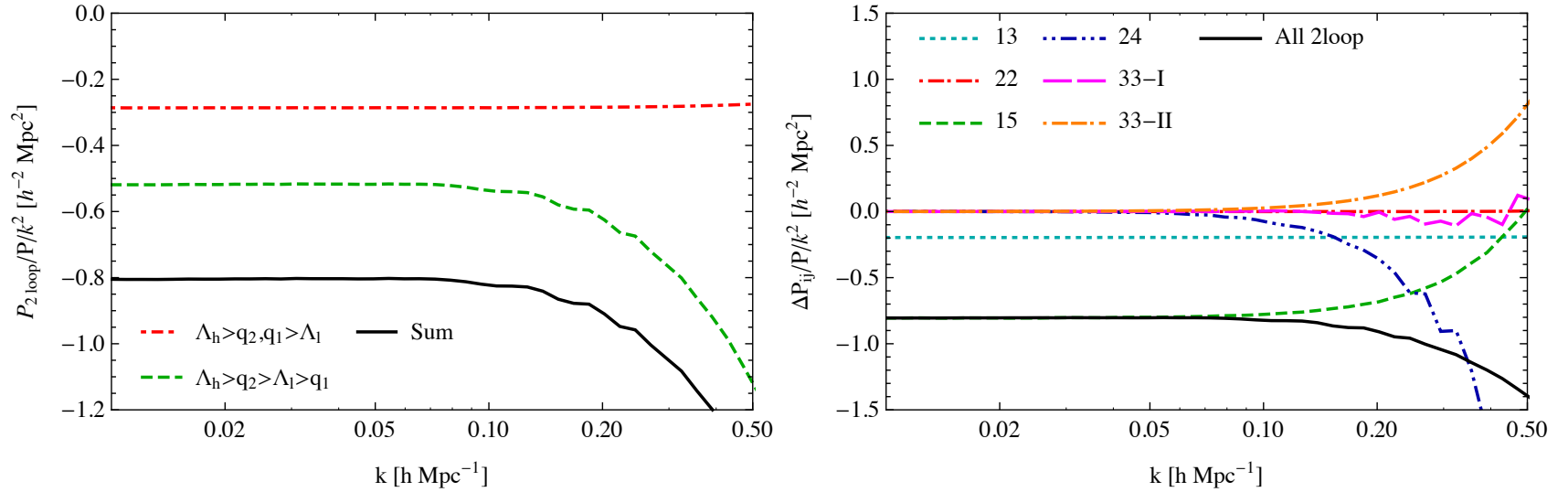


FIG. 3. Effect of changing the cut-off from  $\Lambda_h = 5 h\text{Mpc}^{-1}$  to  $\Lambda_l = 1 h\text{Mpc}^{-1}$  for the one and two loop calculations normalized by  $k^2 P$ . *Left panel:* Contributions from the low-high and high-high terms (single- and double-hard). The mixed term clearly dominates the  $k^2 P$  part and also the deviations from this behavior. *Right panel:* Contributions from the separate diagrams. At the one loop level  $P_{13}$  leads to a  $k^2 P$  contributions, whereas the  $k^4$  contribution from  $P_{22}$  is suppressed.  $P_{15}$  dominates the  $k^2 P$  part but for the deviations from this scaling, there is a cancellation between  $P_{15}$ ,  $P_{33-II}$  and  $P_{24}$ . Like  $P_{22}$  in the one loop case, the  $k^4$  term arising from  $P_{33-I}$  is suppressed.

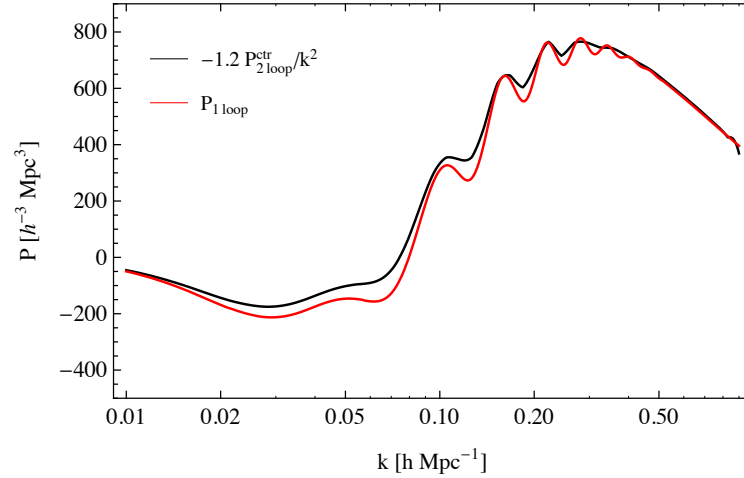


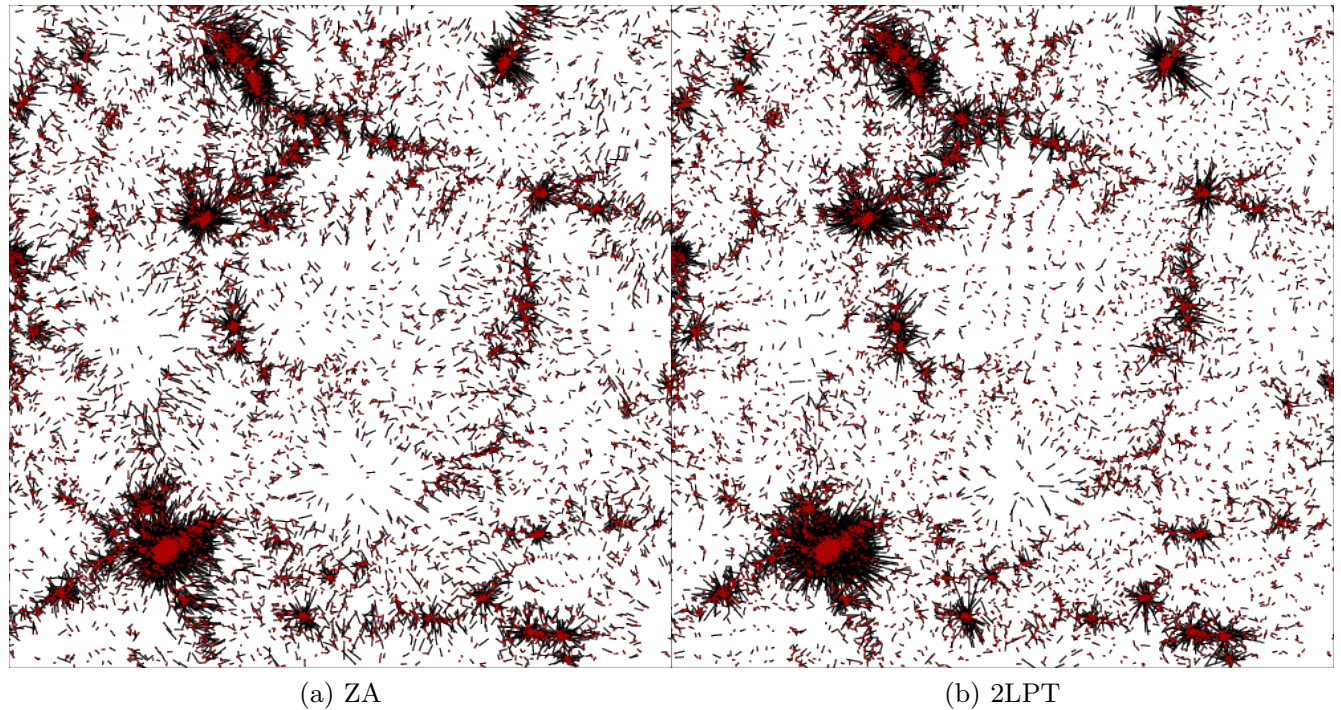
FIG. 4. Comparison between the two-loop counterterm deduced from the divergencies and the one-loop power spectrum weighted by wavenumber squared. We see that the explicit calculation of the two loop counterterms  $\bar{P}_{\text{ctr},2\text{loop}}$  is proportional to the naive estimate  $k^2 P_{1\text{loop}}$ .

$$P_{13}^{q_1 \rightarrow \infty} = -k^2 P \underbrace{\frac{61}{630} \int_{\mathbf{q}} \frac{P(\mathbf{q})}{q^2}}_{l^2 \equiv \frac{61}{210} \sigma_d^2} + k^4 P \frac{2}{105} \int_{\mathbf{q}} \frac{P(\mathbf{q})}{q^4} + \dots$$

$$P_{\text{ctr}} = \alpha \left[ 2P_{13}^{q_1 \rightarrow \infty} + 2\bar{P}_{15}^{q_1 \rightarrow \infty} + 2P_{24}^{q_1 \rightarrow \infty} + P_{33-II}^{q_1 \rightarrow \infty} \right]$$

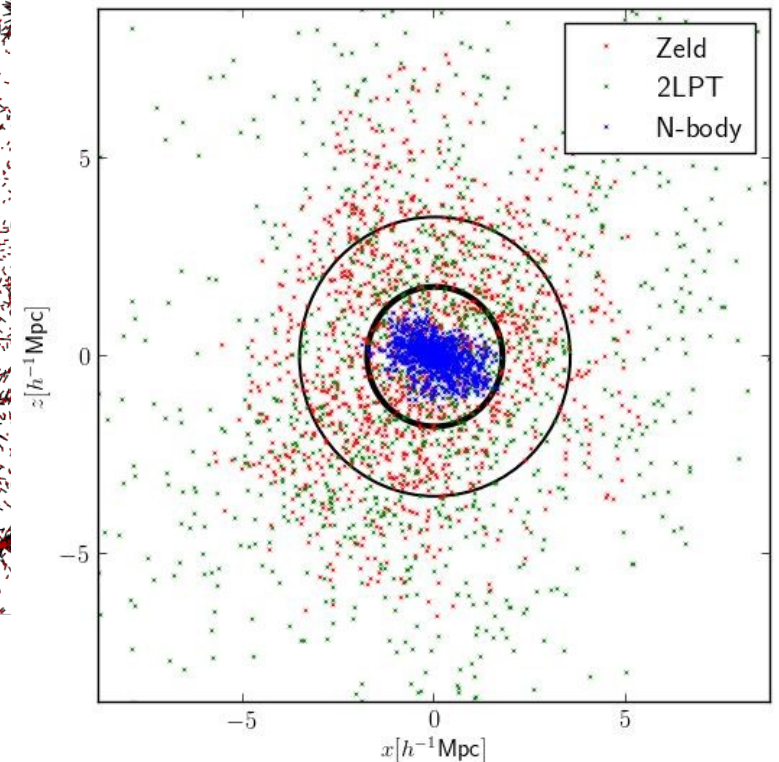
$$P_{\text{ctr,simple}} = -k^2 l^2 \left[ P_{11} + P_{1\text{loop}} \right].$$

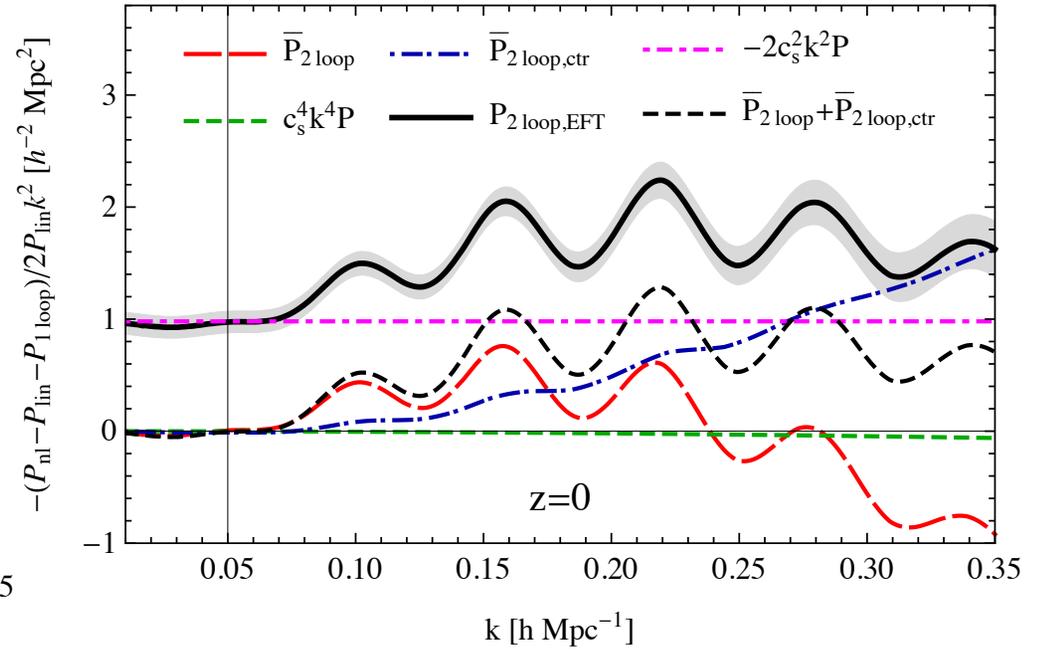
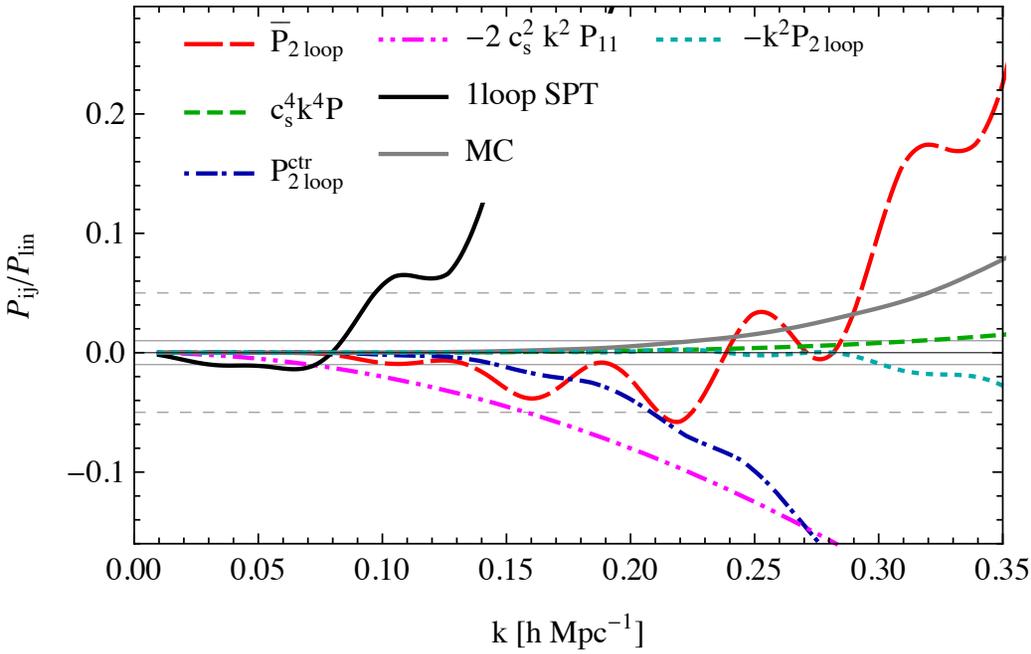
# Example of particle trajectories



We expect that the EFT parameters are mostly correcting the mistakes of PT, in full solution the halo is much smaller than the halo in PT.

EFT parameters are not properties of the fluid but depend on the approximate solution.



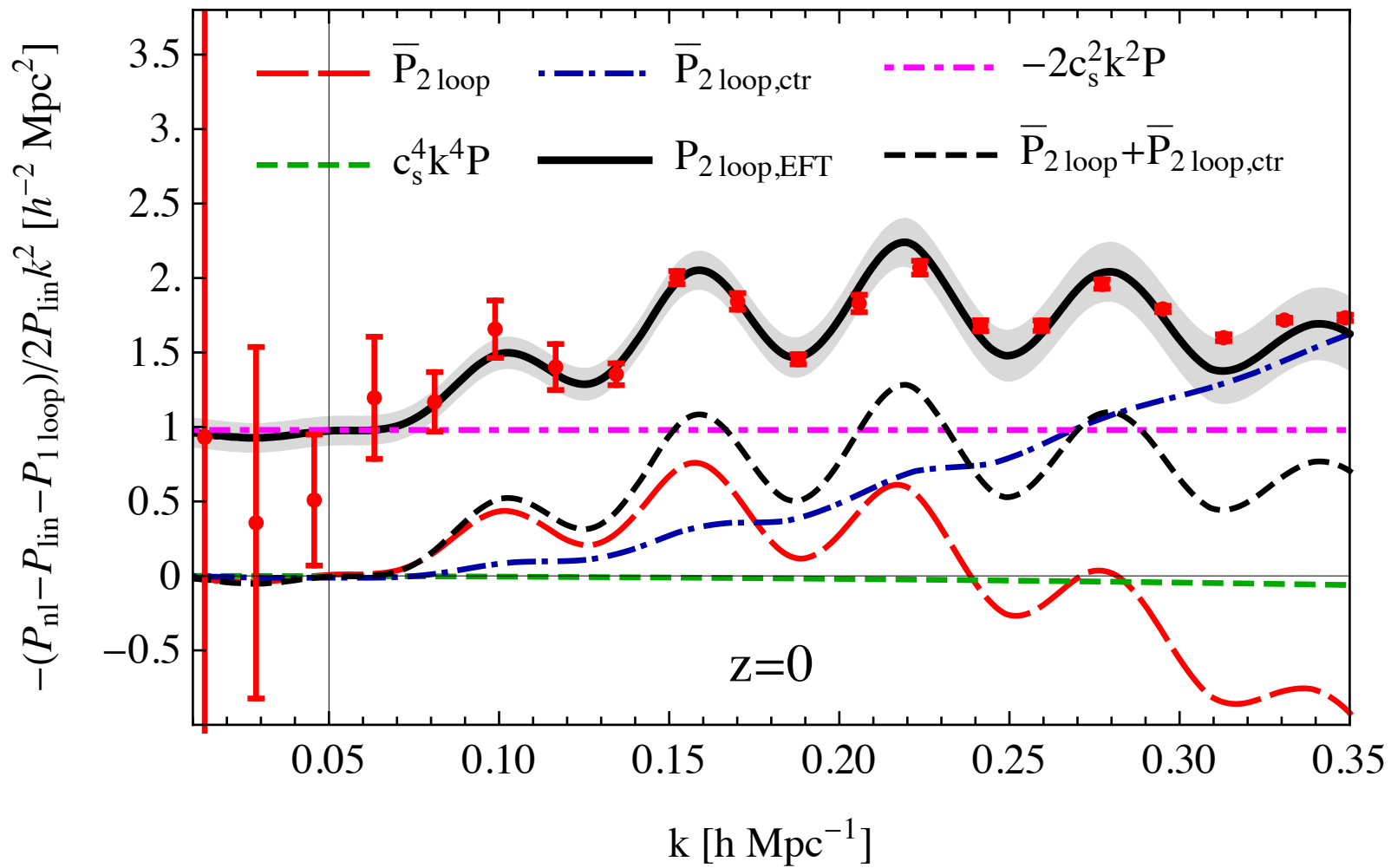


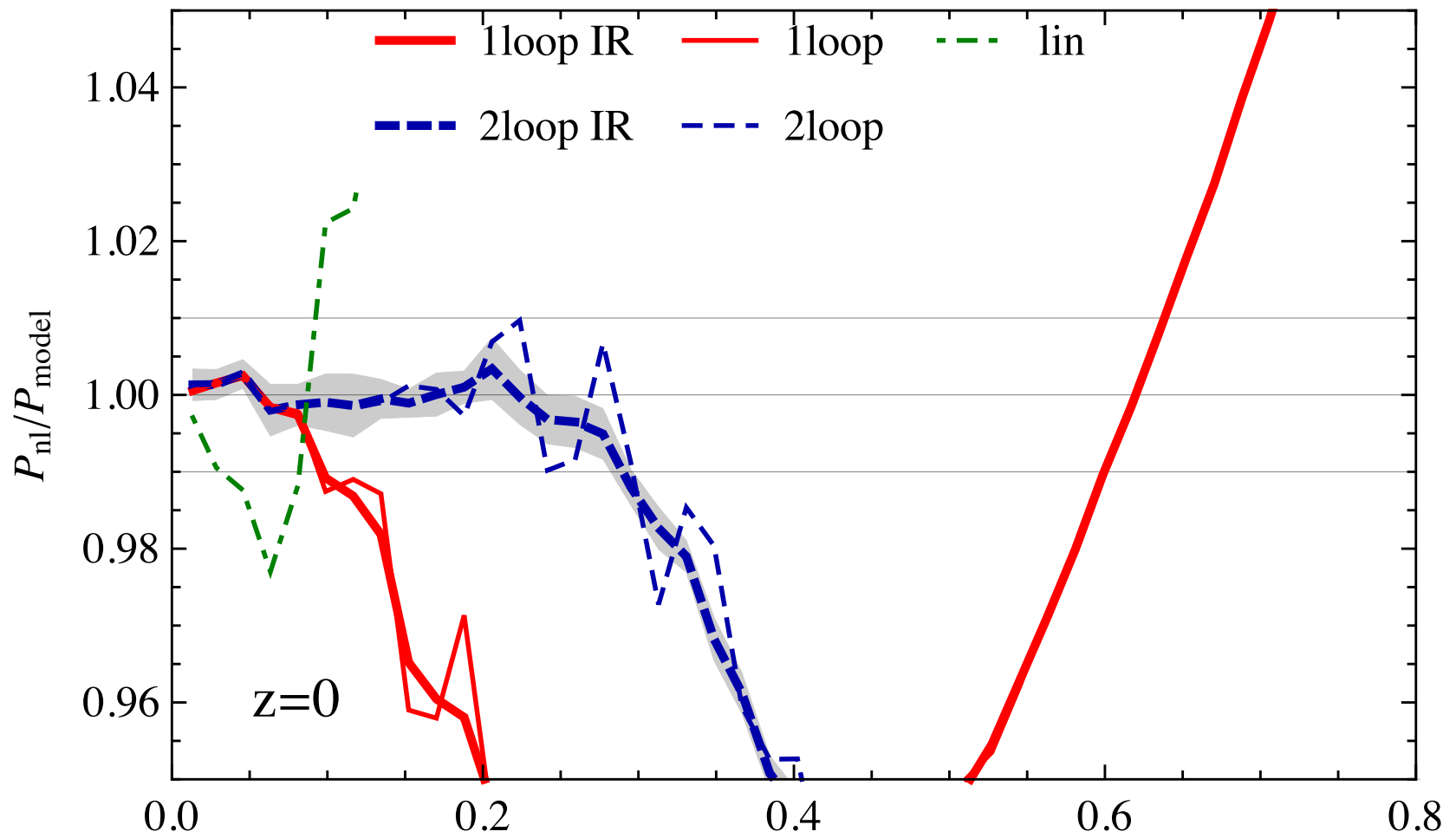
$$P = P_{11} + P_{1\text{loop}} + P_{\text{ctr},1\text{loop}} + \bar{P}_{2\text{loop}} + P_{\text{ctr},2\text{loop}}.$$

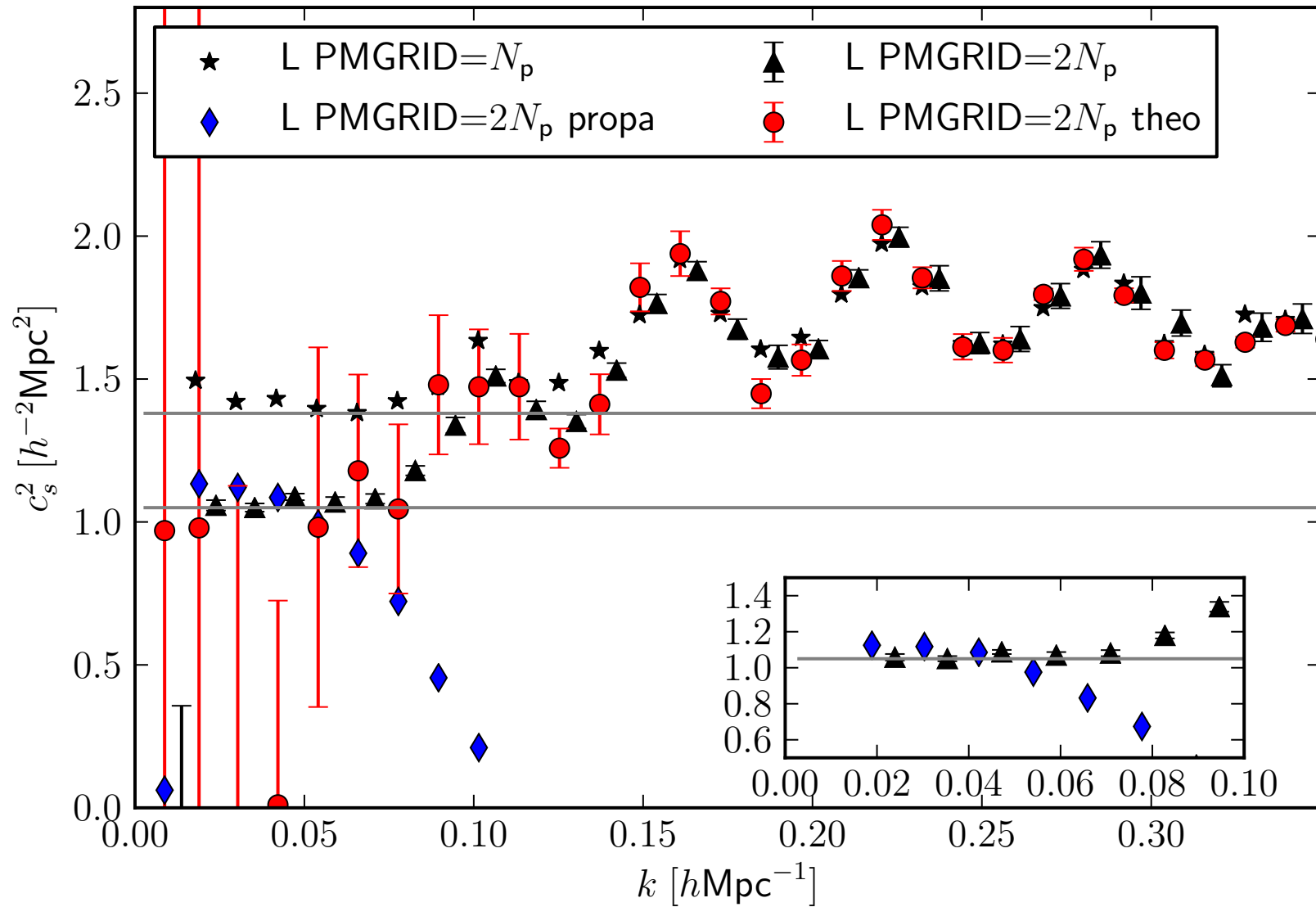
$$\frac{P}{P_{11}} - 1 = \frac{P_{1\text{loop}} + P_{\text{ctr},1\text{loop}} + \bar{P}_{2\text{loop}} + P_{\text{ctr},2\text{loop}}}{P_{11}}$$

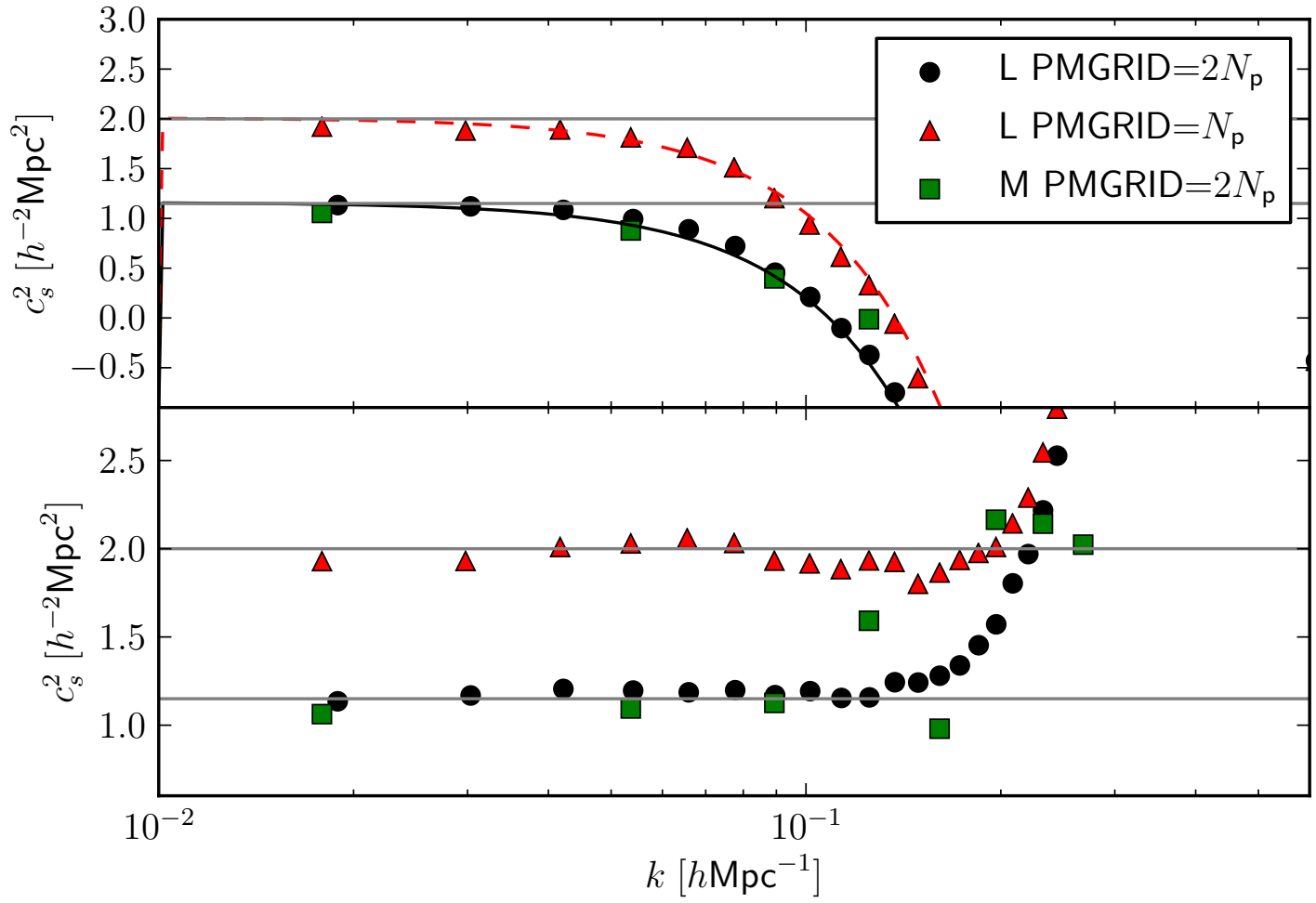
$$-\frac{P - P_{11} - P_{1\text{loop}}}{2k^2 P_{11}} = c_s^2 - \frac{\bar{P}_{2\text{loop}} + P_{\text{ctr},2\text{loop}}}{2k^2 P_{11}}.$$

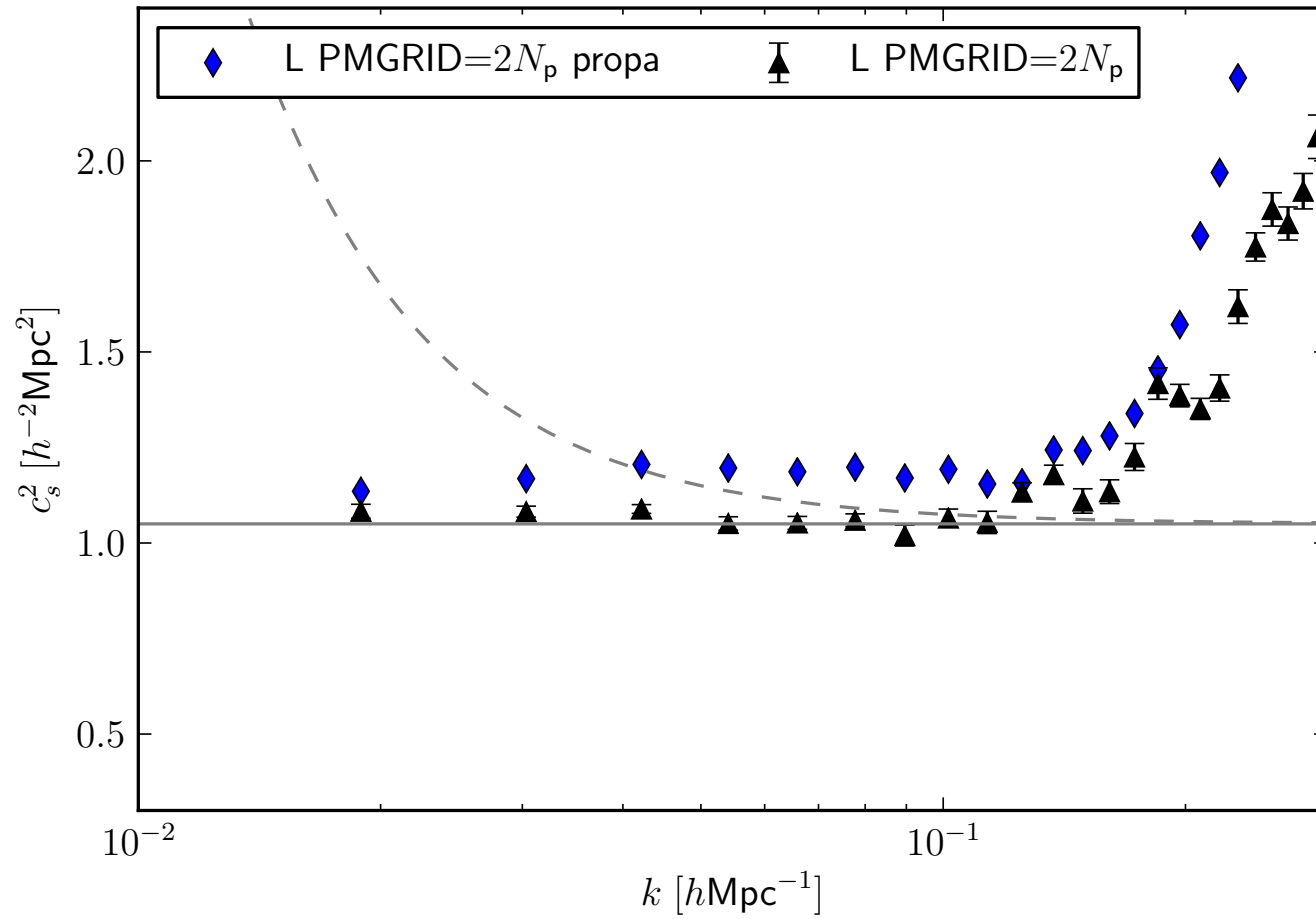
$$\Delta c_s^2 = \frac{\Delta P}{P} \frac{1}{2k^2} \sim \frac{\Delta P/P}{2\%} \left( \frac{k}{0.1 \text{ hMpc}^{-1}} \right)^{-2} h^{-2} \text{Mpc}^2 \sim \frac{\Delta P/P}{0.2\%} \left( \frac{k}{0.03 \text{ hMpc}^{-1}} \right)^{-2} h^{-2} \text{Mpc}^2$$











# Comparison without cosmic variance

Transfer functions:

	$a_1$	$a_2$	$a_3$	$a_4$	$a_5$
tree	11				
1-loop	13	22			
2-loop	15	24	33		
3-loop	17	26	35	44	
4-loop	19	28	37	46	55

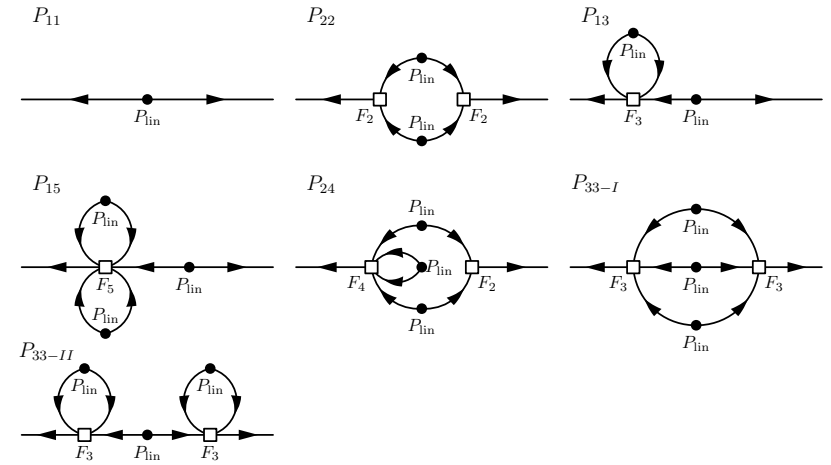


FIG. 1. Diagrams for the tree level, one- and two-loop expressions of the SPT power spectrum.

$$\phi_{ntLPT}(\mathbf{k}) = a_1(k)\phi^{(1)}(\mathbf{k}) + \dots + a_n(k)\phi^{(n)}(\mathbf{k}).$$

$$\phi_{1-loop\ EFT} = (1 + \alpha k^2) \phi^{(1)} + \phi^{(2)} + \phi^{(3)}$$

These can be measured without cosmic variance

$$\phi_{ntLPT}(\mathbf{k}) = a_1(k)\phi^{(1)}(\mathbf{k}) + \dots + a_n(k)\phi^{(n)}(\mathbf{k}) + \phi_{stoch}$$

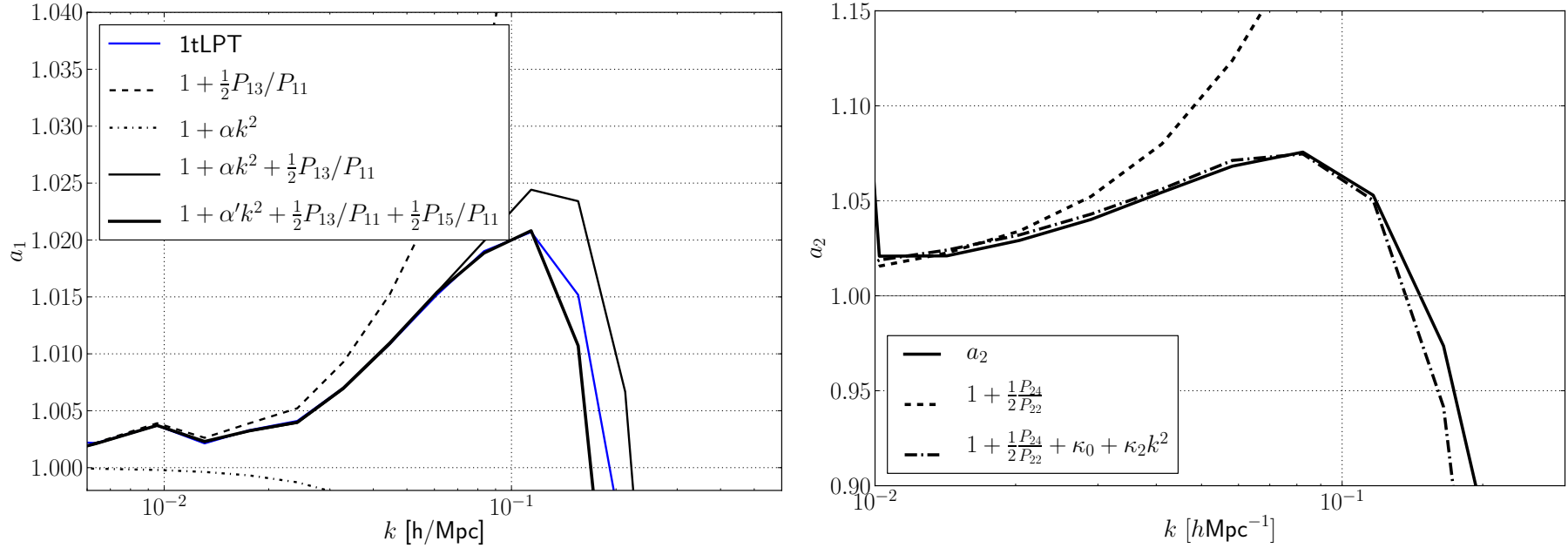
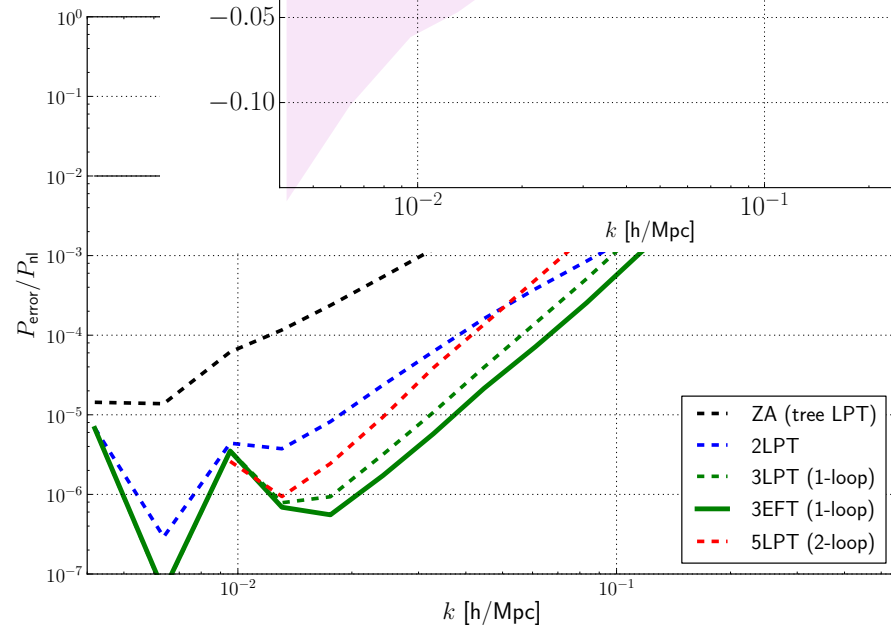
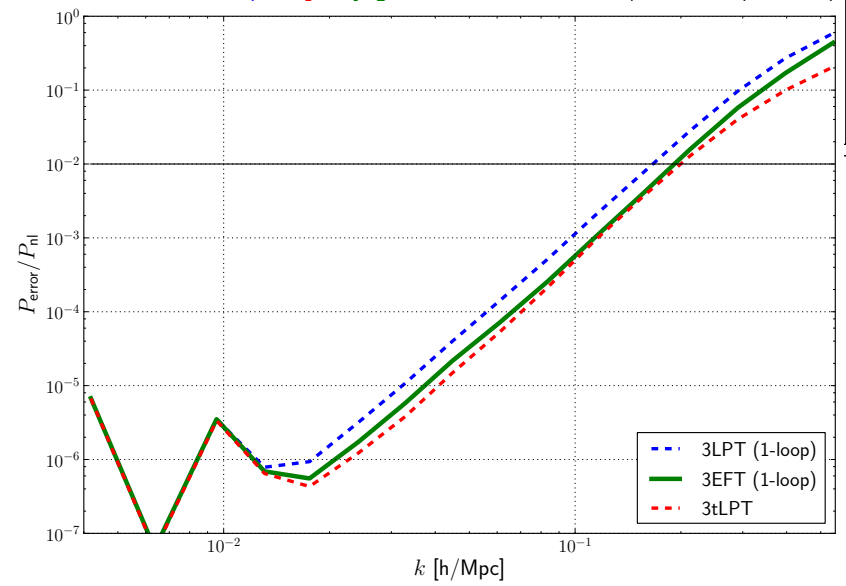
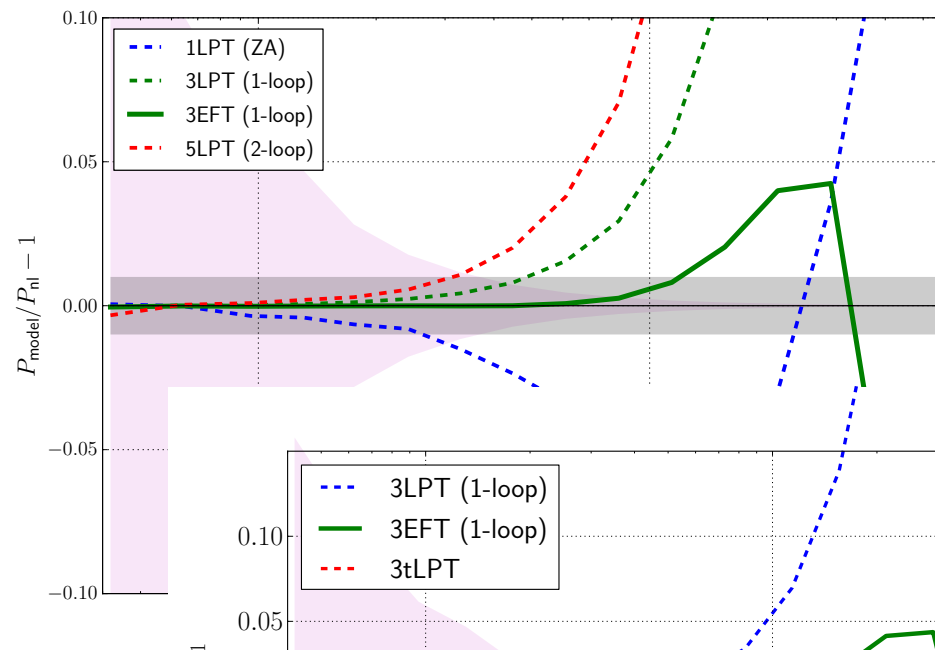
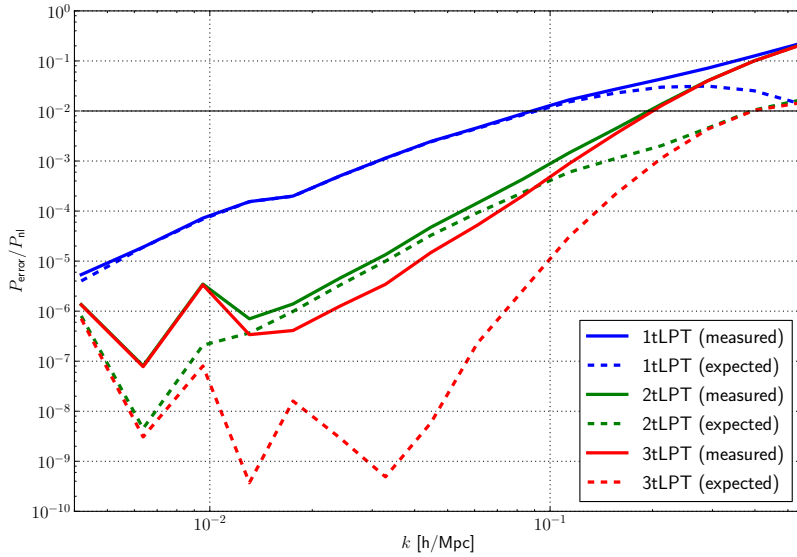


**Figure 19.** *Left panel:* Transfer function  $a_1^\perp$  of the 1tLPT model. Adding  $P_{15}$  modifies the value of  $\alpha$ , as expected, and improves the agreement. *Right panel:* Transfer function  $a_2^\perp$  of the 1tLPT model. We clearly see a percent level deviation on the largest scales, that is accounted for by adding  $P_{24}/P_{22}/2$  to the model for this term. The latter however over predicts the enhancement in the mildly non-linear regime, which is in turn fixed by the EFT counter terms  $E_{2,i}$ . As we pointed out before, they lead to  $k^0$  and  $k^2$  corrections through  $P_{22}/P_{22}$ .

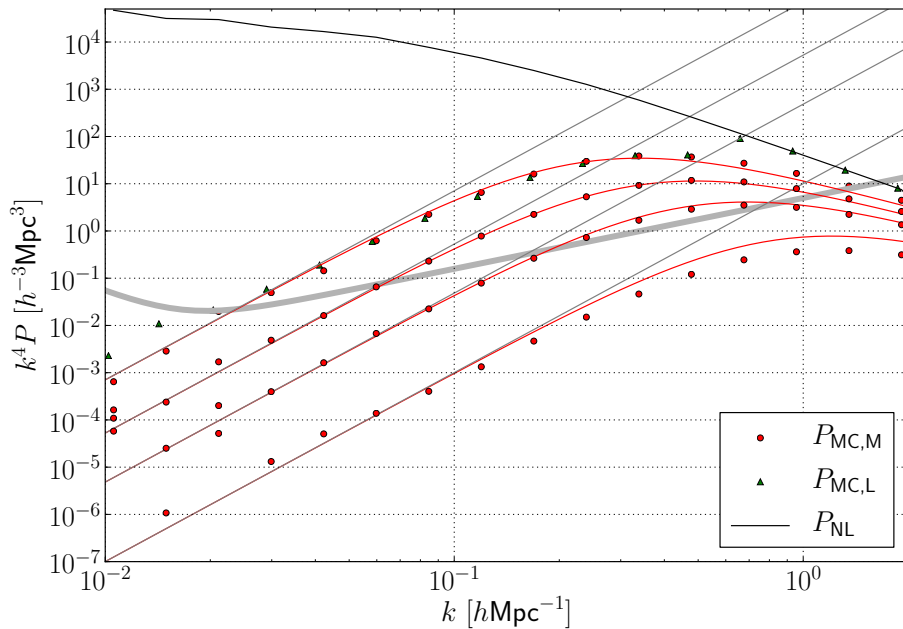


# Stochastic term:



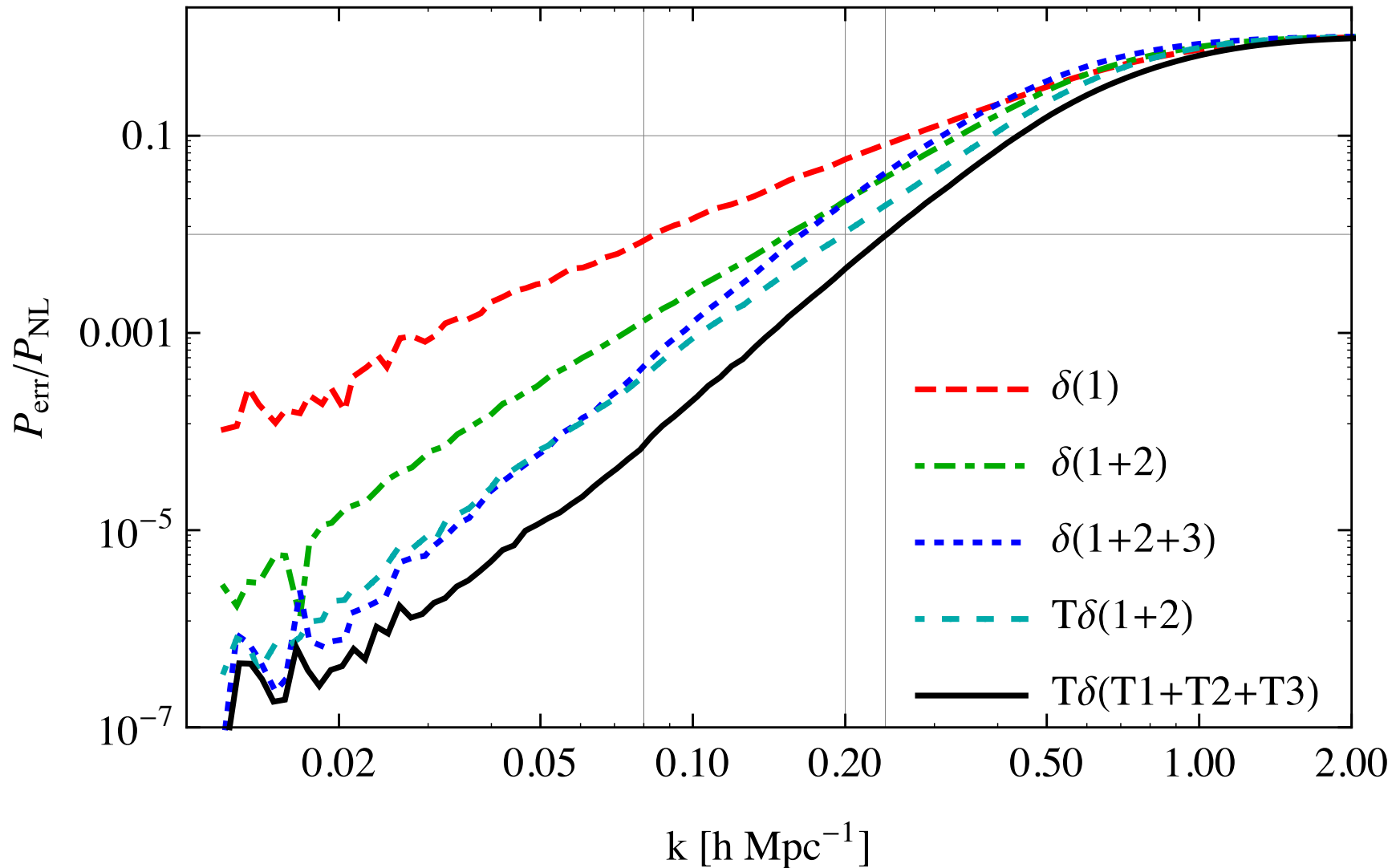
	$a_1$	$a_2$	$a_3$	$a_4$	$a_5$
tree	11				
1-loop	13	22			
2-loop	15	24	33		
3-loop	17	26	35	44	
4-loop	19	28	37	46	55

$$\phi_{ntLPT}(\mathbf{k}) = a_1(k)\phi^{(1)}(\mathbf{k}) + \dots + a_n(k)\phi^{(n)}(\mathbf{k}) + \phi_{\text{stoch}}$$



$$\sigma_{\text{stoch},h}^2 = \int dm \frac{dn}{dm} m \left( 2R_{\text{vir}}(m) \right)^2 / \int dm \frac{dn}{dm} m$$

**Eulerian results**: What happens if we use the displacement to compute the density?



Again the EFT tells you constraints the shape of the transfer functions

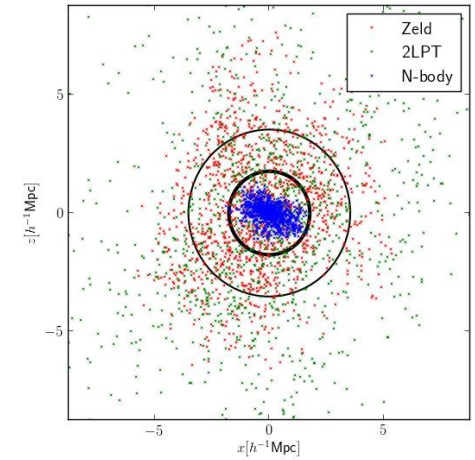
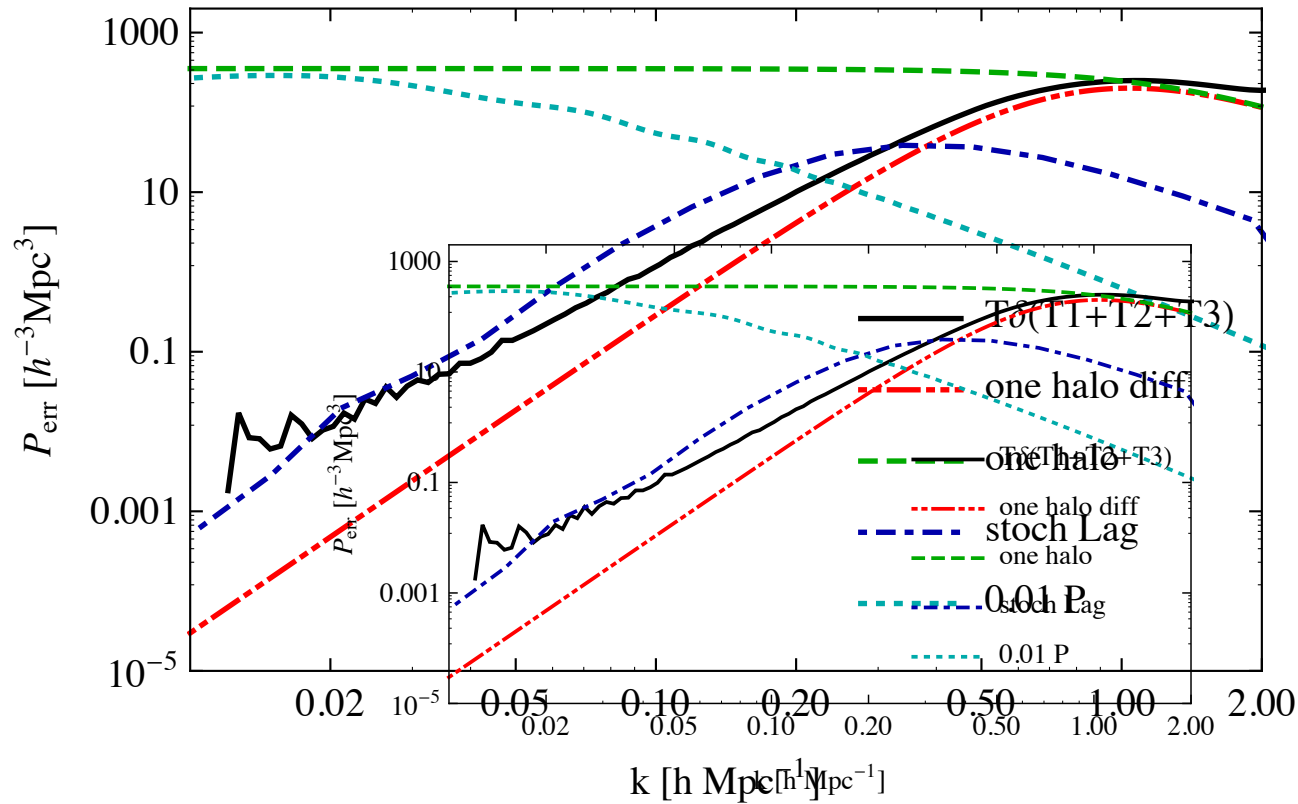


**Figure 9.** Power spectrum of the non-linear one halo term Eq. (5.10) extracted from the simulations and the one halo term of the profile difference between the simulation and 1LPT Eq. (5.12). The gray line shows 1% of the linear power spectrum. We can clearly see that the profile differences amount to percent level corrections to the linear power spectrum at  $k \approx 0.3 \text{ hMpc}^{-1}$ . We also show the stochastic term in Lagrangian space and Eulerian space. The Eulerian stochastic term is larger than the profile difference on large scales but approaches it at  $k \approx 1 \text{ hMpc}^{-1}$ .

Stochastic contribution probably is at the percent level at  $k=0.2$  probably shape is not  $k^4$ .

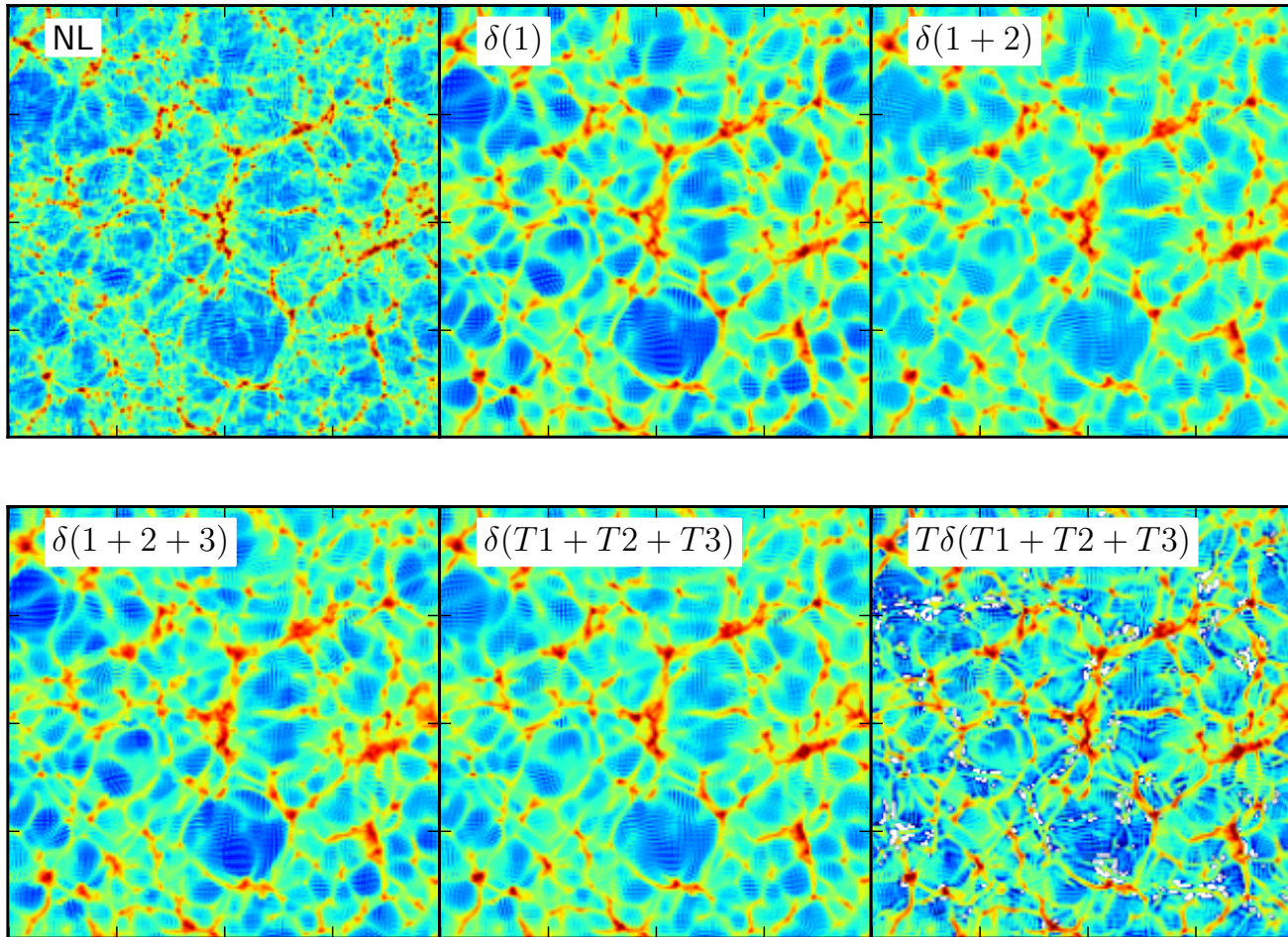


**Figure 7.** Non linear transformation of the density field in a patch of  $300 h^{-1}\text{Mpc}$  length and  $15 h^{-1}\text{Mpc}$  depth.

Transfer function try to fix the fact that the PT solution is too smooth. The mistake is on scales larger than the virial radius but smaller than the Lagrangian radius.

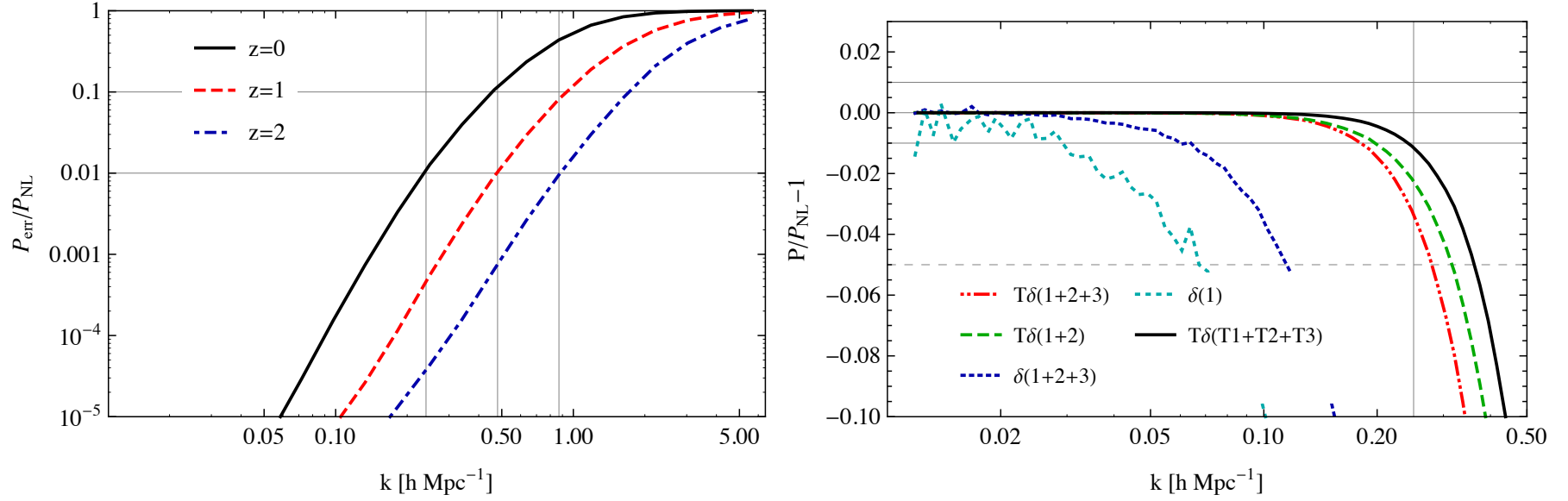


**Figure 6.** *Left panel:* Ratio of the best possible EFT power spectrum to the non-linear power spectrum as a function of redshift. We indicate the 1% and 10% accuracy lines and mark the crossing of the 1%-threshold by vertical lines, whose wavenumbers are given in Tab. 1. *Right panel:* Ratio of the perturbative model with and without transfer functions and the non-linear power spectrum at  $z = 0$ .

## Comparison with simulations

- Comparison can be made without cosmic variance. Agreement is extremely good.
- It can be used to test simulations on large scales. Easy to spot errors in simulations.
- Improve on linear growth factor without having to do many time steps. Non conservation of momentum.
- Errors in simulations can be characterized in the same way. We should routinely report and have a theory of the errors in simulations as a function of sim parameters

# Counter terms for two loops

$$\begin{aligned}
 \langle \delta^{ct} \delta^{SPT} \rangle &= l_1^2 k^2 (P(k) + P_{22}(k) + 2P_{13}(k) + \bar{P}_{22}(k) + 2\bar{P}_{13}(k)) \\
 &+ 2k^3 \int \frac{dr r^2}{(2\pi)^2} P(kr) \int_{-1}^1 dx P(k\sqrt{y(r,x)}) \left[ \frac{3}{14} \frac{(1-x^2)}{y(r,x)} + \frac{1}{2} \frac{(1-rx)x}{ry(r,x)} \right] \\
 &\times \left[ k^2 l_{2a}^2 + k^2 l_{2b}^2 \frac{(1-x^2)}{y(r,x)} + k^2 l_{2c}^2 \frac{(1-rx)(x-r)x}{ry(r,x)} \right] \\
 &+ P(k) 2k^3 \int \frac{dr r^2}{(2\pi)^2} P(kr) \\
 &\times \int_{-1}^1 dx \left[ k^2 \bar{l}_{2c}^2 \frac{x^2(1-rx)(1-x^2)}{y(r,x)} + k^2 l_{3a}^2 \frac{(1-x^2)^2}{y(r,x)} + k^2 l_{3b}^2 \frac{rx(1-x^2)^2}{y(r,x)} \right].
 \end{aligned}$$

$$y(r, x) = 1 + r^2 - 2rx$$

$$P_{22}(k) = \int_p 2F_2^2(\mathbf{p}, \mathbf{k} - \mathbf{p}) P(p) P(|\mathbf{k} - \mathbf{p}|)$$

$$P_{13}(k) = P(k) \int_p 3F_3(\mathbf{k}, \mathbf{p}, -\mathbf{p}) P(p)$$

$$\bar{P}_{22}(k) = \int_p 4F_2^2(\mathbf{p}, \mathbf{k} - \mathbf{p}) \frac{\mathbf{p} \cdot (\mathbf{p} - \mathbf{k})}{k^2} P(p) P(|\mathbf{k} - \mathbf{p}|)$$

$$\bar{P}_{13}(k) = P(k) \int_p 3F_3(\mathbf{k}, \mathbf{p}, -\mathbf{p}) \frac{p^2}{k^2} P(p),$$

# Equations of motion

$$\begin{aligned}\partial_\tau \delta + \partial_i [(1 + \delta)v^i] &= 0, \\ \partial_\tau v^i + \mathcal{H}v^i + \partial^i \phi + v^j \partial_j v^i &= -\frac{1}{\rho} \partial_j \tau^{ij} \equiv -\frac{1}{(1 + \delta)} \partial_j \tilde{\tau}^{ij} \\ \Delta \phi &= \frac{3}{2} \mathcal{H}^2 \Omega_m \delta. \\ \ddot{\psi}^i + \mathcal{H}\dot{\psi}^i + \frac{\partial}{\partial x^i} \phi &= -\frac{1}{(1 + \delta)} \frac{\partial}{\partial x^j} \tilde{\tau}^{ij},\end{aligned}$$

$$\begin{aligned}\mathbf{x}_{fl}(\mathbf{x}, \tau; \tau') + \int_{\tau'}^{\tau} d\tau'' \mathbf{v}(\mathbf{x}_{fl}(\mathbf{x}, \tau; \tau''), \tau'') &= \mathbf{x}. \\ \boldsymbol{\psi}(\mathbf{x}, \tau) &= \mathbf{x} - \mathbf{q}(\mathbf{x}, \tau). \\ \mathbf{q}(\mathbf{x}, \tau) &\equiv \mathbf{x}_{fl}(\mathbf{x}, \tau; 0)\end{aligned}$$

## Counter terms

$$\begin{aligned}\bar{\tau}_{ij}^{(1)} &\propto \delta_{ij} \psi_{k,k}^{(1)} = \delta_{ij} \phi_{,kk}^{(1)} \\ \bar{\tau}_{ij}^{(1)} &\propto \psi_{i,j}^{(1)} = \phi_{,ij}^{(1)}.\end{aligned}$$

$$\bar{\tau}_{ij}^{(2)} \propto b_1 \delta_{ij} (\phi_{,kk}^{(1)})^2 + b_2 \delta_{ij} \phi_{,kl}^{(1)} \phi_{,kl}^{(1)} + b_3 \phi_{,ik}^{(1)} \phi_{,kj}^{(1)}$$

$$\begin{aligned}\bar{\tau}_{ij}^{(3)} &\propto c_1 \delta_{ij} (\phi_{,kk}^{(1)})^3 + c_2 \phi_{,ik}^{(1)} \phi_{,kj}^{(1)} \phi_{,mm}^{(1)} + c_3 \delta_{ij} \phi_{,kl}^{(1)} \phi_{,kl}^{(1)} \phi_{,mm}^{(1)} + c_4 \phi_{,ik}^{(1)} \phi_{,kl}^{(1)} \phi_{,lj}^{(1)} \\ &+ c_5 \delta_{ij} \phi_{,kl}^{(1)} \phi_{,lm}^{(1)} \phi_{,mk}^{(1)} + c_6 \phi_{,kl}^{(1)} \phi_{,kl}^{(1)} \phi_{,ij}^{(1)} + c_7 \phi_{,ij}^{(1)} \phi_{,mm}^{(1)} \phi_{,nn}^{(1)} \\ &+ \frac{c_8}{2} (\phi_{,ik}^{(1)} \phi_{,kj}^{(2)} + \phi_{,ik}^{(2)} \phi_{,kj}^{(1)}) + c_9 \delta_{ij} \phi_{,kl}^{(1)} \phi_{,kl}^{(2)} \\ &+ c_{10} (\psi_{i,j}^{(3)} + \psi_{j,i}^{(3)})\end{aligned}$$

## Mapping from displacement to density

$$\delta(\mathbf{k}) = \int d^3 q \ e^{i\mathbf{k} \cdot (\mathbf{q} + \boldsymbol{\psi})}$$

$$\delta(\mathbf{k}) = \delta^{SPT}(\mathbf{k}) + \sum_n \frac{i^n}{(n-1)!} \int \frac{d^3 p_1}{(2\pi)^3} \cdots \frac{d^3 p_n}{(2\pi)^3} (2\pi)^3 \delta^D(\mathbf{p}_1 + \cdots + \mathbf{p}_n - \mathbf{k}) \mathbf{k} \cdot \boldsymbol{\psi}^{ct}(\mathbf{p}_1) \mathbf{k} \cdot \boldsymbol{\psi}^{SPT}(\mathbf{p}_2) \cdots \mathbf{k} \cdot \boldsymbol{\psi}^{SPT}(\mathbf{p}_n)$$

- The time dependence of the counter term matters when including it into the equations of motion to compute terms linear in the counter term but higher order in perturbations.
- If the divergence of stress tensor is the gradient of a scalar then counter terms generated by the equations of motions are degenerate with higher order counter terms for two additional orders.
- For 2-loop counter terms this means that only one of the quadratic counter terms need to be followed through the equation of motion. Even in this case, at the level of the power spectrum these terms are degenerate with cubic counter terms.
- There are higher order counter terms associated with a given counter term from the mapping between displacement and density. Those do not depend on the time dependence of the source.

$$\bar{\tau}_{ij}^{(2)} \propto b_1 \delta_{ij} (\phi_{,kk}^{(1)})^2 + b_2 \delta_{ij} \phi_{,kl}^{(1)} \phi_{,kl}^{(1)} + b_3 \phi_{,ik}^{(1)} \phi_{,kj}^{(1)}$$

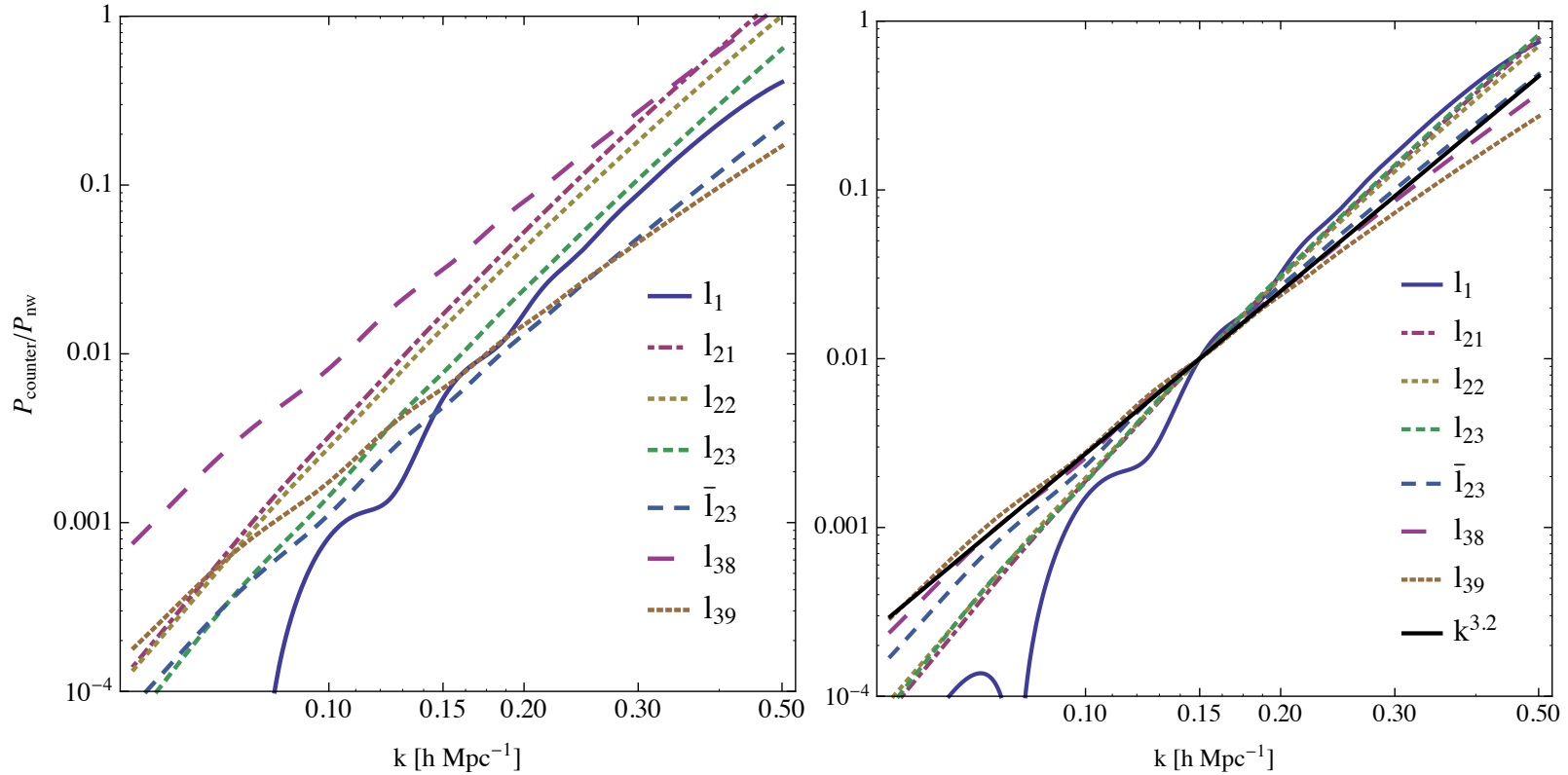
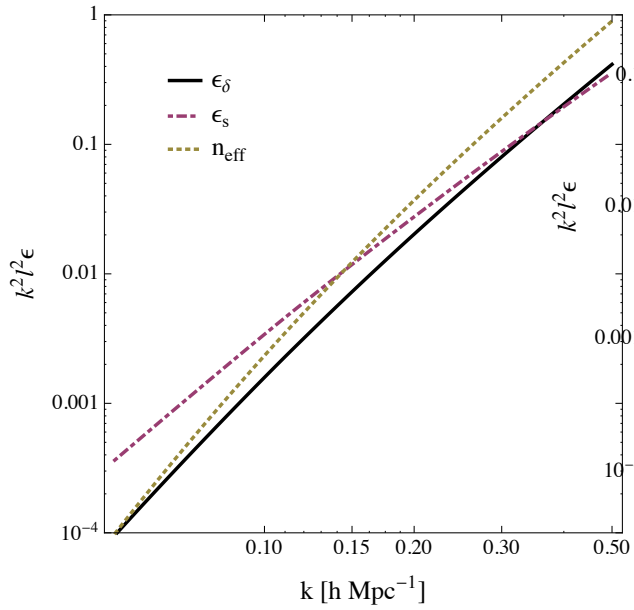


FIG. 1: Left: Two loop counter term contributions for  $l^2 = 1 (h^{-1} \text{Mpc})^2$ . Right: Two loop counter term contributions normalized so that they are 1% of the linear power spectrum at  $k = 0.15 h \text{Mpc}^{-1}$ . We also show a representative power law that roughly captures the scaling of these terms.



$$\epsilon_s = k^2 \int_{q \gg k} \frac{d^3 q}{(2\pi)^3} \frac{P(q)}{q^2}$$

$$\epsilon_\delta = \int_{q \ll k} \frac{d^3 q}{(2\pi)^3} P(q)$$

$$n_{eff} = \frac{d \log P}{d \log k}.$$

$$k^2 l^2 \epsilon_\delta \quad k^2 l^2 \epsilon_\delta n_{eff}$$

$$k^2 l^2 \epsilon_s$$

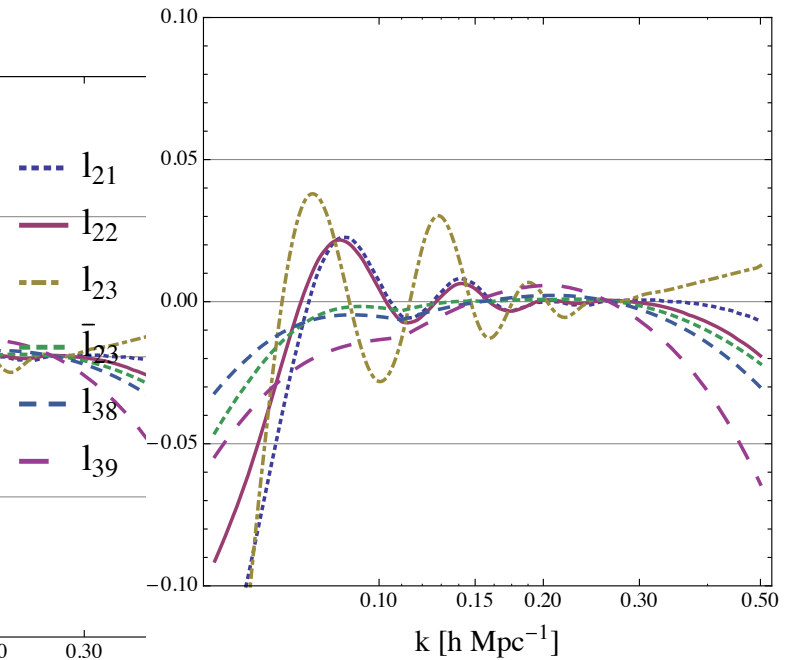
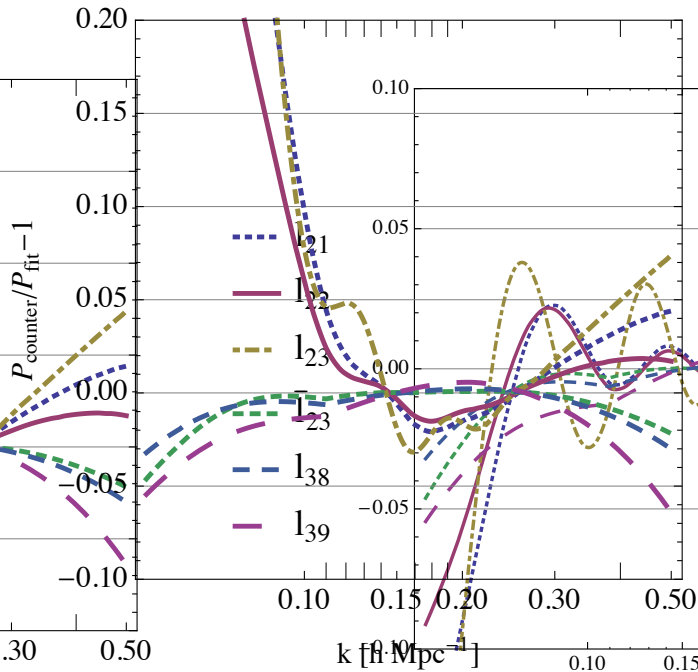


FIG. 3: Left: Fit to the five two loop counter terms using a linear combination of  $k^2 P_{\epsilon_\delta}$  and  $k^2 P_{\epsilon_s}$ . Right: adding a term proportional to  $k^2 n_{eff} P_{\epsilon_\delta}$ .

# Theoretical errors & neutrino masses

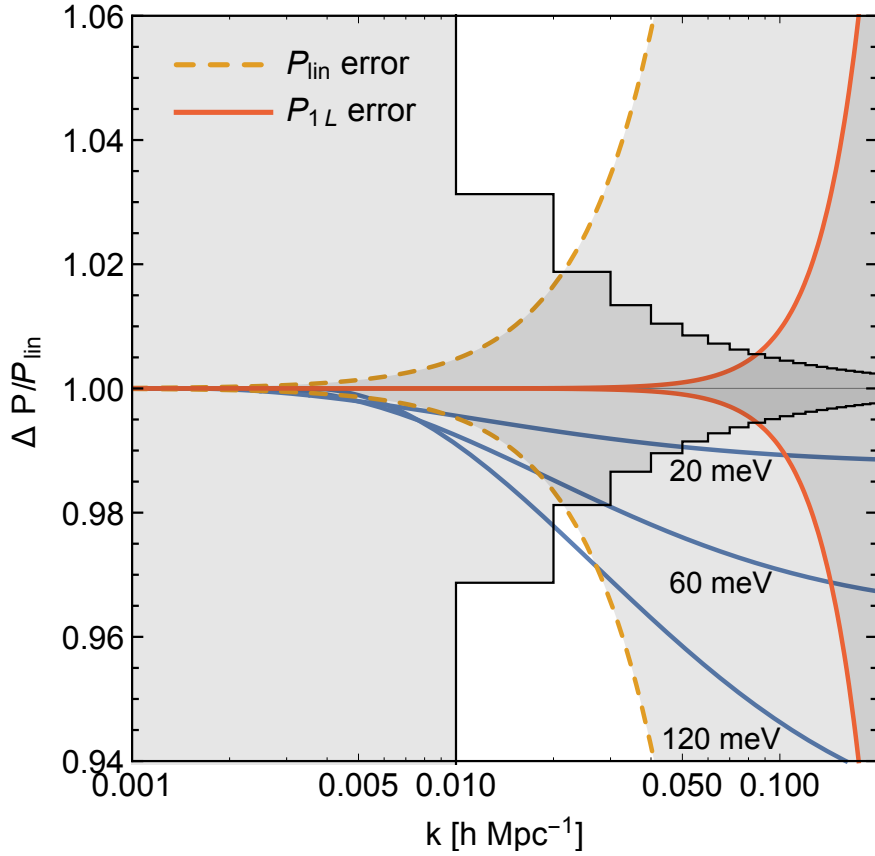
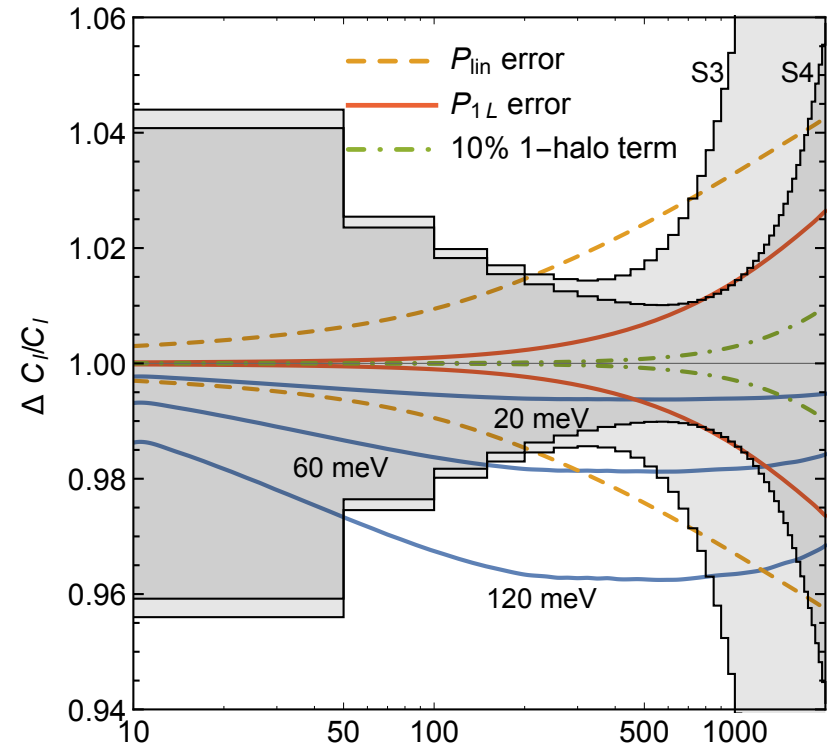
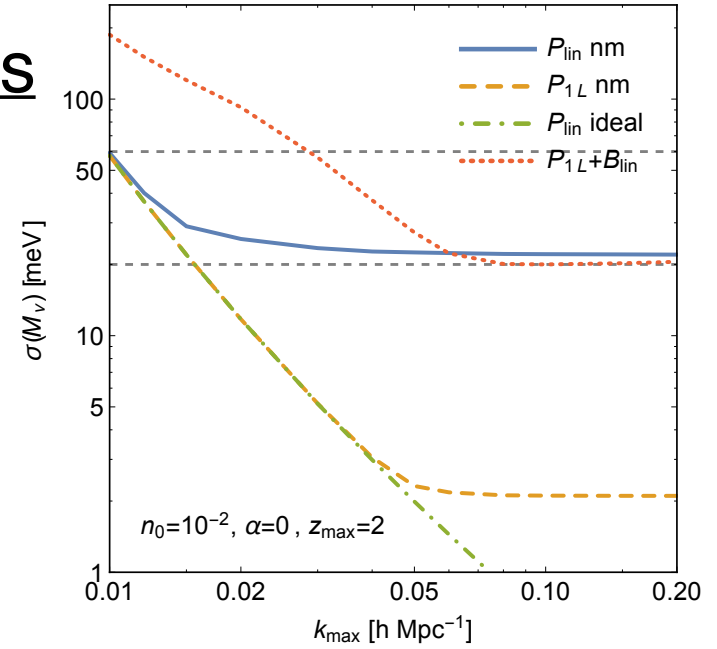


FIG. 2: Theoretical errors for the linear theory and one-loop power spectrum (see Eq. (42)) as a function of  $k$ . The cosmic variance is plotted for the redshift bin  $1 < z < 2$ . Three solid lines are relative suppression of the power spectrum for three different  $M_\nu$ .



# Theoretical errors & non-Gaussianity

$$f_{\text{NL}}^{\text{loc.}} = 0.8 \pm 5.0, \quad f_{\text{NL}}^{\text{eq.}} = -4 \pm 43, \quad (68\% \text{ CL}).$$

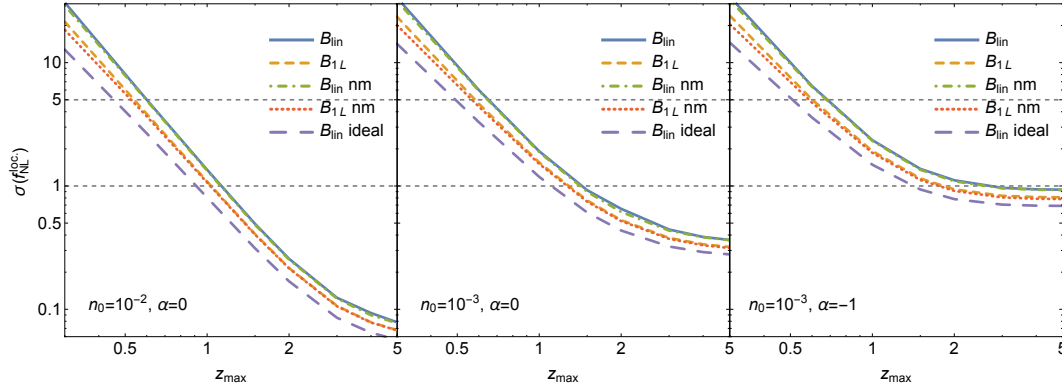


FIG. 7: One sigma error bar on  $f_{\text{NL}}^{\text{loc.}}$  as a function of the maximal redshift  $z_{\text{max}}$ . Two horizontal lines correspond to  $f_{\text{NL}}^{\text{loc.}} = 5$  (the current strongest bound from the CMB) and  $f_{\text{NL}}^{\text{loc.}} = 1$  which is an interesting theoretical threshold. Each panel shows the constraints with and without marginalization over the EFT and bias parameters. Different lines correspond to different combinations of the tree-level and the one-loop bispectrum and corresponding errors. The effects of the marginalization are minimal, given that the local shape is orthogonal to gravitational contributions. We also plot as a reference a line for the ideal case of no theoretical error and no marginalization.

Improvement seems likely

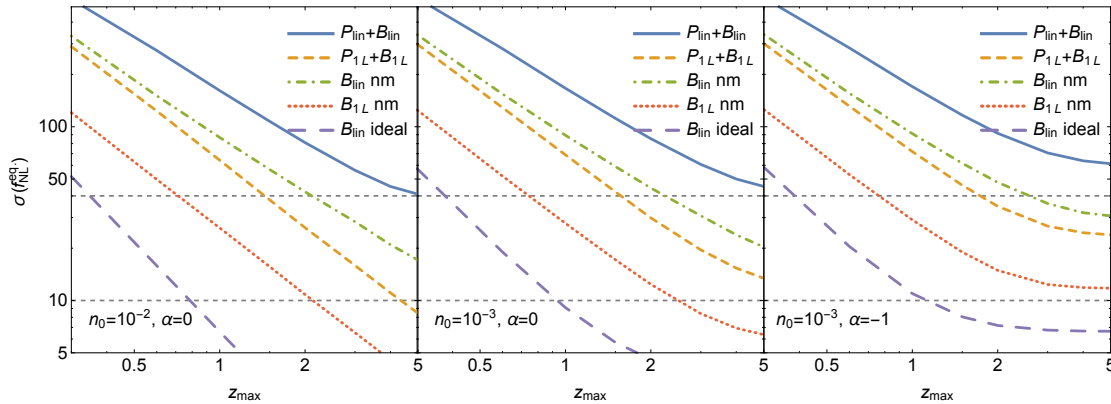


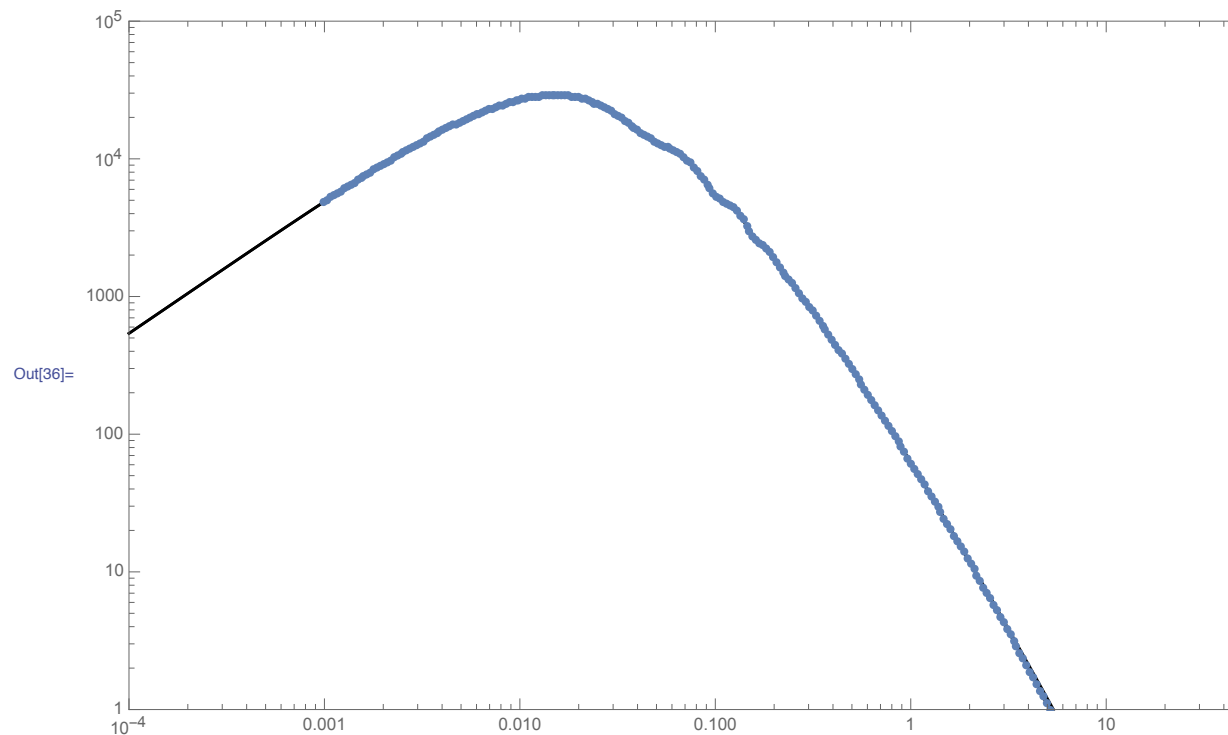
FIG. 6: One sigma error bar on  $f_{\text{NL}}^{\text{eq.}}$  as a function of the maximal redshift  $z_{\text{max}}$ . Two horizontal lines correspond to  $f_{\text{NL}}^{\text{eq.}} = 40$  (the current strongest bound from the CMB) and  $f_{\text{NL}}^{\text{eq.}} = 10$ . Each panel shows the constraints with and without marginalization over the EFT and bias parameters. Different lines correspond to different combinations of the tree-level and the one-loop power spectrum and bispectrum. As a reference we also plot a line for the ideal case with no theoretical error and no marginalization.

Improvement looks very difficult

# Fast computations

```
In[4]:= FpowerFFT[bias_, kvec_, kpivot_, plin_, cmout_] := Module[{nn, Pvec}, nn = Dimensions[kvec][[1]];  
Pvec = Table[plin[kvec[[i]]], {i, 1, nn}];  
cmout = Fourier[Pvec / (kvec / kpivot)bias, FourierParameters → {-1, 1}];]
```

```
In[5]:= powerrecFFT[b_, kvec_, kpivot_, cm_, powerout_] := Module[{bias, pk}, Dimensions[cm][[1]];  
bias =  $\left(\frac{kvec}{kpivot}\right)^b$  ;  
pk = Re[bias Fourier[cm, FourierParameters → {1, -1}]]; powerout = Transpose[{kvec, pk}];]
```



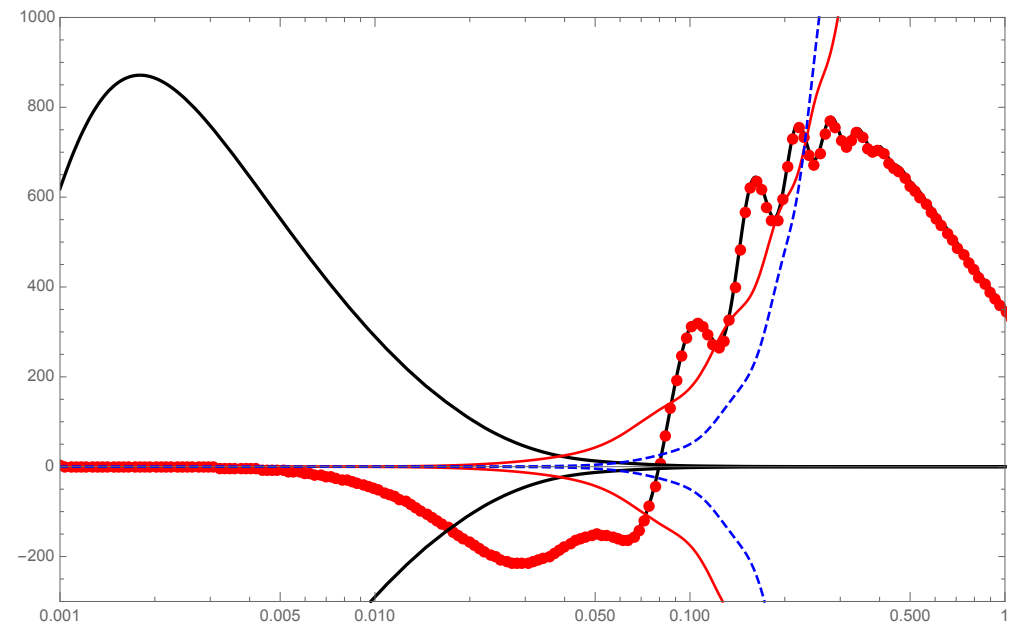
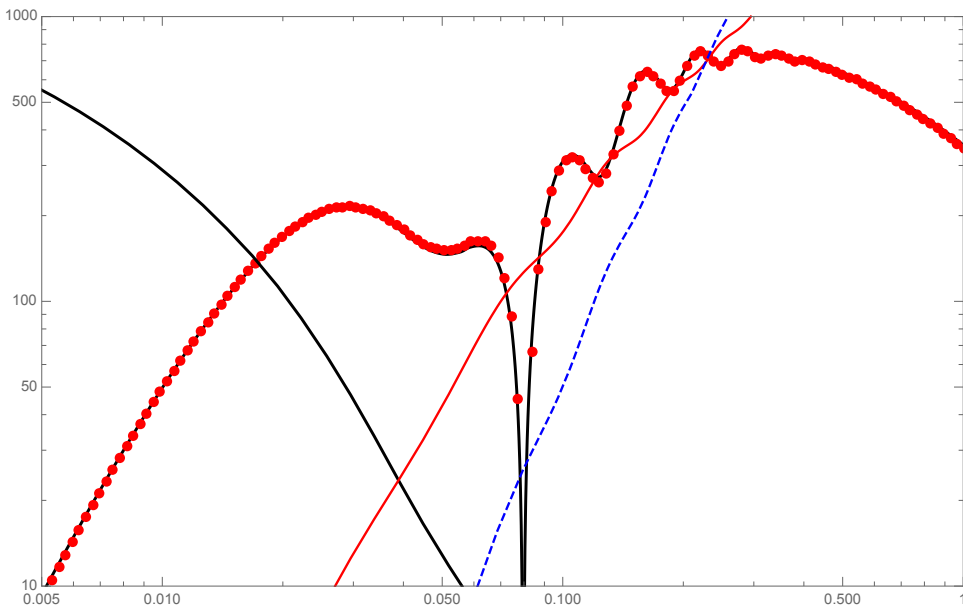
$$\text{P13feynfin}[n1_, k_] = -\frac{k^{3+n1} (-2 + 9 n1) \text{Csc}\left[\frac{1}{2} (3 + n1) \pi\right]}{224 \text{Gamma}\left[2 - \frac{n1}{2}\right] \text{Gamma}\left[4 + \frac{n1}{2}\right]};$$

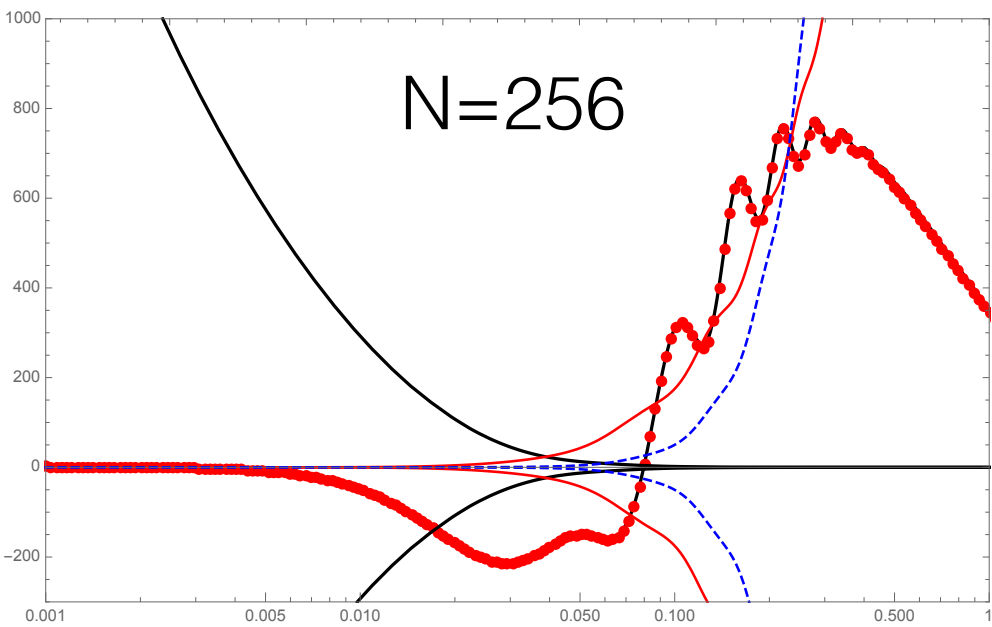
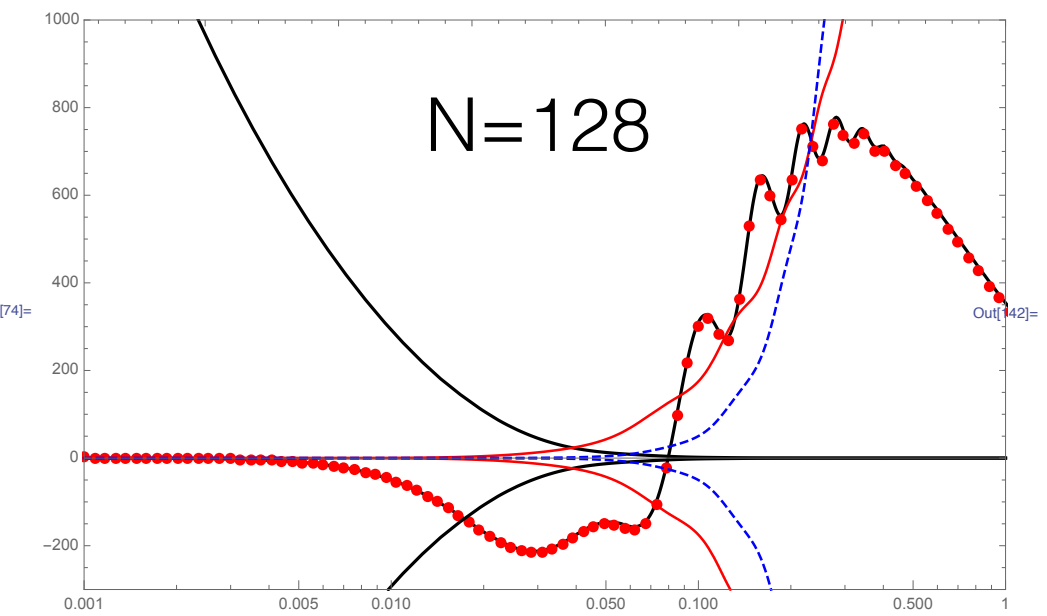
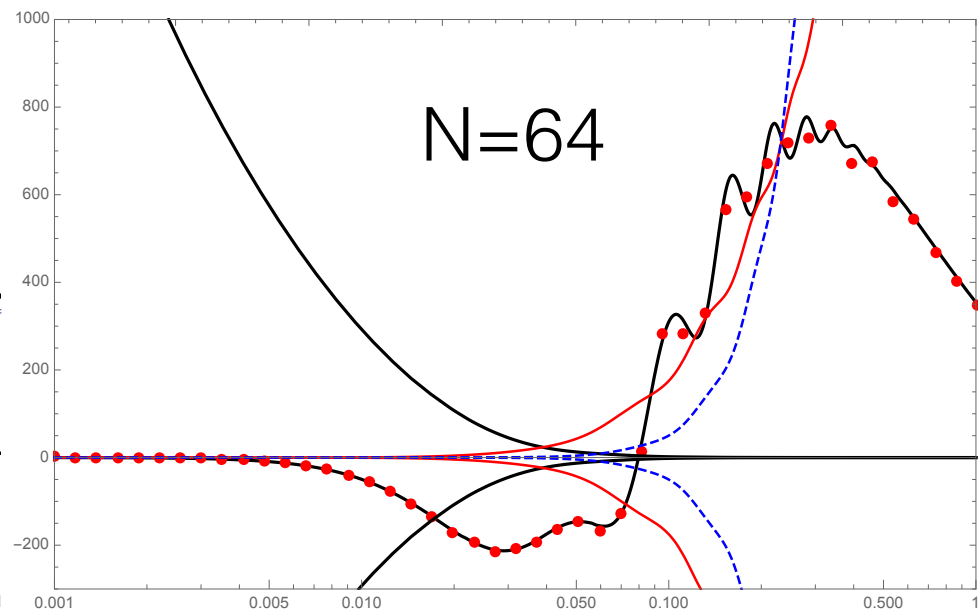
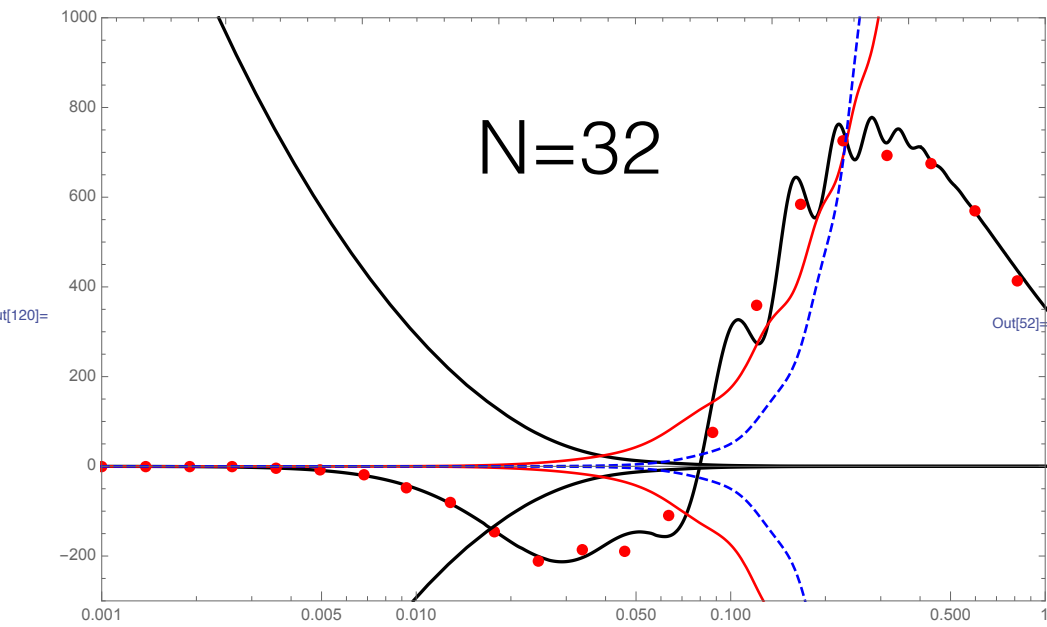
`P22feynfin[n1_, n2_, k_] =`

$$\left( k^{3+n1+n2} \left( 1296 + 49 n1^3 (-3 + n2) + 1944 (-4 + n1 + n2) + 9 \left( 1560 + 5 n1 (-166 + 21 n1) - 830 n2 + 226 n1 n2 + 105 n2^2 \right) + 7 n1^2 (142 + n2 (-85 + 14 n2)) - (-2 + n2) (808 + 7 n2 (-100 + 21 n2)) + n1 (-2208 + n2 (2000 + 7 n2 (-85 + 7 n2))) \right) + 3 \left( -2904 + 49 n1^3 + 7 n1^2 (-101 + 29 n2) + n2 (2574 + 7 n2 (-101 + 7 n2)) + n1 (2574 + 7 n2 (-206 + 29 n2)) \right) \text{Gamma}\left[\frac{1+n1}{2}\right] \text{Gamma}\left[\frac{1}{2} (1 - n1 - n2)\right] \text{Gamma}\left[\frac{1+n2}{2}\right] \right) / \left( 12544 \pi^{3/2} \text{Gamma}\left[2 - \frac{n1}{2}\right] \text{Gamma}\left[2 - \frac{n2}{2}\right] \text{Gamma}\left[\frac{1}{2} (6 + n1 + n2)\right] \right);$$

`p13recFFT[b_, kvec_, kpivot_, cm_, ppcutvec_, p13out_] :=`

```
Module[{dfreq, intfreq, freq, nn, prefactor, cmp13, p13k}, nn = Dimensions[cm][[1]];
dfreq = 2 π / Log[kvec[[nn]] / kvec[[1]]] (nn - 1) / nn; intfreq = Table[{i - 1 - UnitStep[i - nn / 2 - 2] nn}, {i, 1, nn}];
freq = intfreq dfreq; prefactor = ppcutvec kvec3+b (1 / kpivotb); cmp13 = Table[cm[[i]] P13feynfin[b - I freq[[i]], 1], {i, 1, nn}];
p13k = Re[prefactor Fourier[cmp13, FourierParameters -> {1, -1}]]; p13out = Transpose[{kvec, p13k}];]
```





$$J(v_1, v_2, v_3) \equiv \int \frac{d^d \mathbf{q}}{(q^2)^{v_1} [(k_1 - \mathbf{q})^2]^{v_2} [(k_2 - \mathbf{q})^2]^{v_3}}.$$

$$\begin{aligned}
J(v_1, v_2, v_3) = & \frac{\pi^{d/2} k_1^{d-2v_{123}}}{\Gamma(v_1)\Gamma(v_2)\Gamma(v_3)\Gamma(d-v_{123})} \left[ \Gamma(v_3)\Gamma\left(v_{123} - \frac{d}{2}\right) F_4\left(v_3, v_{123} - \frac{d}{2}; 1 + v_{23} - \frac{d}{2}, 1 + v_{13} - \frac{d}{2}; x, y\right) \right. \\
& \times \Gamma\left(\frac{d}{2} - v_{13}\right)\Gamma\left(\frac{d}{2} - v_{23}\right) + y^{d/2-v_{13}}\Gamma(v_2)\Gamma\left(\frac{d}{2} - v_1\right) F_4\left(v_2, \frac{d}{2} - v_1; 1 + v_{23} - \frac{d}{2}, 1 - v_{13} + \frac{d}{2}; x, y\right) \\
& \times \Gamma\left(v_{13} - \frac{d}{2}\right)\Gamma\left(\frac{d}{2} - v_{23}\right) + x^{d/2-v_{23}}\Gamma(v_1)\Gamma\left(\frac{d}{2} - v_2\right) F_4\left(v_1, \frac{d}{2} - v_2; 1 - v_{23} + \frac{d}{2}, 1 + v_{13} - \frac{d}{2}; x, y\right) \\
& \times \Gamma\left(\frac{d}{2} - v_{13}\right)\Gamma\left(v_{23} - \frac{d}{2}\right) + x^{d/2-v_{23}}y^{d/2-v_{13}}\Gamma\left(\frac{d}{2} - v_3\right) F_4\left(d - v_{123}, \frac{d}{2} - v_3; 1 - v_{23} + \frac{d}{2}, 1 - v_{13} + \frac{d}{2}; x, y\right) \\
& \left. \times \Gamma(d - v_{123})\Gamma\left(v_{23} - \frac{d}{2}\right)\Gamma\left(v_{13} - \frac{d}{2}\right) \right], \tag{A3}
\end{aligned}$$

The End